Journal of Fluids and Structures 96 (2020) 103015

Contents lists available at ScienceDirect

Journal of Fluids and Structures

journal homepage: www.elsevier.com/locate/jfs

Experimental study of the self-excited resonance effect on the dynamic lift and flow structure around inline cylinders

Mahmoud Shaaban, Atef Mohany *

Faculty of Engineering and Applied Science, University of Ontario Institute of Technology, Oshawa, Ontario, Canada

ARTICLE INFO

Article history:
Received 4 February 2020
Received in revised form 25 March 2020
Accepted 28 April 2020
Available online 20 May 2020

Keywords:
Inline cylinders
Cross-flow
Shear layer instability
Dynamic lift force
Resonance excitation

ABSTRACT

The excitation of acoustic resonance by air flow around a row of inline cylinders is investigated experimentally using phase-locked particle image velocimetry and direct measurements of the dynamic lift forces. The experiments are performed during self-excited acoustic resonance for arrangements of two, three, four, and five inline cylinders with a spacing ratio $L/D = 2.0$, where L is the center-to-center distance between the cylinders and D is the cylinder diameter, to clarify the effect of increasing the number of cylinders on the resonance mechanism and the characteristics of the periodic flow cycle. The PIV measurements show that increasing the number of cylinders results in weaker and distorted periodic flow structures around the most downstream cylinders. However, the phase and strength of the flow structures within the most upstream gap are minimally affected. Intrinsic flow features, such as gap flow that is observed in some cases, lead to the disruption of the shear layer impingement on downstream cylinders. Moreover, direct measurements of the dynamic lift forces on all cylinders simultaneously identified the upstream gap as the location where most of the energy exchange between the flow and the acoustic fields occurs. Decomposition of the dynamic lift force with respect to the acoustic pressure revealed that the distorted flow structures were accompanied by weaker, sometimes negative, contribution to the acoustic resonance excitation. The findings presented in this article explain the observation that for inline configurations of cylinders, as well as inline tube bundles, increasing the number of cylinders in the flow direction does not result in stronger resonance, and demonstrate that countermeasures for resonance excitation should target the most upstream rows of cylinders.

© 2020 Elsevier Ltd. All rights reserved.

* Corresponding author.
E-mail address: atef.mohany@uoit.ca (A. Mohany).

https://doi.org/10.1016/j.jfluidstructs.2020.103015
0889-9746/© 2020 Elsevier Ltd. All rights reserved.

Nomenclature

B	Test section span
H	Test section height
L	Cylinder center-to-center spacing
D	Cylinder diameter
Re	Reynolds number
H	Test section height
$P*$	Normalized acoustic pressure
f	Frequency
U_r	Reduced flow velocity
U_∞	Upstream flow velocity
f_a	Acoustic mode frequency
P_{rms}	Root mean square acoustic pressure
ρ	Air density
H	Test section height
ω	Vorticity
H	Test section height
x, y, and z	Streamwise, transverse, and spanwise coordinates; respectively
u_a	Acoustic particle velocity
d_a	Acoustic particle displacement
ϕ_p	Phase angle of acoustic pressure
F_L	Dynamic lift force
p	Instantaneous acoustic pressure
u_a	Acoustic particle velocity
φ	Phase angle of dynamic lift force with respect to acoustic pressure
u_a	Acoustic particle velocity
c_l'	Dynamic lift coefficient amplitude
θ	Phase angle of dynamic lift force of two successive cylinders
u_a	Acoustic particle velocity
c_l	Instantaneous dynamic lift coefficient
c_{dh}	Dynamic lift coefficient amplitude out-of-phase with acoustic pressure
c_{mh}	Dynamic lift coefficient amplitude in-phase with acoustic pressure

1. Introduction

The arrangement of inline cylinders in cross-flow is an essential part in a wide variety of engineering components, such as industrial heat exchangers. Under certain conditions, periodic perturbations in the flow around inline cylinders have been reported to cause acoustic resonance of severe sound pressure levels that interrupts operation, poses environmental hazards and eventually leads to mechanical failures (Eisinger et al., 1996). Due to the increased demand on energy, upgrading the flow capacities in power plant components has been a common practice. As a result, incidents related to acoustic resonance excitation by flow around arrangements of cylinders have been increasingly reported since mid-twentieth century (Owen, 1965). The coupled flow-acoustic field can sustain strong resonance excitation, which has materialized in applications that involve flows in confined systems, including tubes in industrial heat exchangers (Ziada, 2010; Arafa and Mohany, 2015, 2019), nuclear reactor components (DeBoo et al., 2006), flow over cavities (Shaaban and Mohany, 2015; Omer et al., 2016a), jet engine compressors (Koch, 2009; Liu et al., 2018), piping systems (Chen and Sturchler, 1977; Karthik et al., 2003; Wang and Liu, 2019), and many other applications. Better understanding of the physics underlying the excitation mechanism of acoustic resonance by separated unsteady flows can help alleviate its dangerous effects during the design stage.

The excitation mechanisms by which flow can give rise to acoustic resonance share the following general description. Free shear flows may become unstable and result in fluctuations of pressure and velocity. If these fluctuations occur at a frequency close to that of an acoustic mode with a proper orientation, they can drive the particle velocity of the acoustic mode. The excited acoustic mode resonates, and the frequency of the flow perturbations "locks-in" the frequency of the acoustic mode. The acoustic field then strengthens the fluctuations in the flow field, and the perturbations resulting from an oscillating flow pattern engage in a feedback mechanism with the acoustic field sustaining a strong resonance excitation (Ziada, 2006). Typical examples of this mechanism include the excitation of acoustic resonance by perturbations observed behind a single cylinder (Hong et al., 2020), separated shear layers past symmetrically located side

branches (Oshkai and Velikorodny, 2013), planar gas jet impinging normally on a flat surface (Arthurs and Ziada, 2012), channel branches (Wang et al., 2019, 2020), and impinging shear layers over rectangular cavities (Ziada et al., 2003; Omer et al., 2016b). Production of sound by vortex shedding can be modeled as a dipole sound source in the direction of the dominant dynamic force, i.e. in the lift direction (Inoue and Hatakeyama, 2002). During resonance excitation, the acoustic field enhances the strength of vorticity and increases its correlation length along the span of the cylinder, which is bound to increase the amplitude of the dynamic lift force (Blevins, 1985). Moreover, the Lighthill–Curle aeroacoustic analogy postulates that the interaction of an aeroacoustic field at rigid surfaces represents a dipole sound source, which is the main acoustic energy source in resonant cases (Curle, 1955). Therefore, the amplitude and phase of the dynamic lift force are direct indicators of the energy exchange mechanism that feeds the resonant field and sustains high acoustic pressures.

Excitation of acoustic resonance by flow around inline tube bundles was investigated by Ziada and Oengören (1992) who pointed out that symmetric vortices are shed in the gaps between cylinders. They identified a pulsating flow pattern where the vorticity shedding in the gaps between cylinders leads to the excitation of acoustic resonance in inline tube bundles. To simplify the investigated flow patterns and interactions, Blevins and Bressler (1993) investigated the case of a single cylinder, observing that an acoustic mode of a confining duct around an isolated cylinder can couple with the vorticity shedding downstream of the cylinder when both occur at the same frequency, leading to excitation of a strong acoustic resonance. Mohany and Ziada (2005) reported that the configuration of two tandem cylinders is susceptible to the same mechanism of excitation as inline tube bundles. For two tandem cylinders, the gap flow instabilities were able to couple with the acoustic mode at flow velocities much lower than necessary for frequency coincidence, resulting in an earlier episode of resonance referred to as "pre-coincidence resonance". By identifying the location of the acoustic source(s) during resonance, Mohany and Ziada (2009b) concluded that the resonance excitation by flow instabilities within the gap is closer in nature to the excitation mechanism of inline tube bundles.

Pre-coincidence resonance may pose a threat that is over-looked when tests are done on cylinders of small diameters, as it results in resonance at lower flow velocities than that predicted at the frequency coincidence (Mohany and Ziada, 2005). In a subsequent study, Mohany and Ziada (2009a) investigated the effect of the cylinder diameter on the excitation of pre-coincidence resonance by two tandem cylinders at a fixed spacing ratio. They showed that a minimum cylinder diameter is required for the excitation of pre-coincidence resonance. This interesting behavior arises as a result of the effect of the cylinder diameter on; the reattachment length of the shear layer in the gap between the cylinders, the dynamic head of the flow at resonance conditions, the acoustic particle velocity of the acoustic mode, and the acoustic radiation losses. Shaaban and Mohany (2019a) observed that the flow around an inline row of multiple cylinders can excite pre-coincidence acoustic resonance. Moreover, Shaaban and Mohany (2019b) showed that Rossiter-like modes in the gaps between successive cylinders may excite resonance for evenly-spaced three inline cylinders. They also reported that under certain conditions, the same mechanism may excite resonance for some unevenly-spaced cases. Flow visualizations at resonant and non-resonant conditions indicated that the flow structure in the gaps is crucial to the excitation of acoustic resonance. The identification of the excitation mechanism that is responsible for pre-coincidence resonance is required to model and design counter measures to mitigate the hazards it imposes. Few studies reported experimental data regarding the effects of acoustic resonance on the flow field. Wang et al. (2018) used planar particle image velocimetry to experimentally investigate the influence of acoustic resonance on flow dynamics in a straight channel with coaxial side branches. They showed that vorticity fluctuations and Reynolds shear stresses were increased significantly when subjected to acoustic modulation. Islam and Mohany (2020) experimentally investigated the effect of the fin-to-root diameter ratio on the near wake flow development and vortex shedding characteristics downstream of straight circular finned cylinders using particle image velocimetry (PIV). They reported that the susceptibility of finned cylinders to resonance excitation is associated to a significant reduction in the recirculation zone, in addition to an amplified primary vortex shedding process in the wake of the cylinders. For the case of self-excited resonance, Shaaban and Mohany (2019b) showed a significant change in the patterns of flow field in the gaps between three unevenly-spaced cylinders due to the excitation of acoustic resonance. Measurement of the amplitude and phase of the dynamic lift force are used to investigate the flow-sound interactions leading to excitation of resonance, and to identify flow-surface interactions that sustain resonance in complex structures. The dynamic lift on the surface of a cylinder is the integrated effect of the surrounding flow structures. The phase between this dynamic lift and the acoustic pressure can give an insight into the overall energy exchange mechanism at the dominant frequency. However, direct simultaneous measurements of dynamic forces on cylinders in a resonant flow field can be very challenging to perform. Unlike flow-induced vibration, acoustic resonance often occurs at significantly higher frequencies, which requires the measurement system to have sufficiently high stiffness to ensure that the system has a significantly high mechanical resonance frequency. The typical technique to measure fluctuating forces on cylinders is the use of pressure taps to characterize the force around the circumference of the cylinder (e.g. Gu et al., 2012). However, using such technique, the phase angle information of the lift forces with respect to the acoustic pressure cannot be accurately obtained. Moreover, acoustic resonance induces strong forces at frequencies that may interact with the structural vibration modes of hollow cylinders, and therefore solid, more stiff cylinders are required to prevent that. To overcome this limitation, direct measurements of the fluctuating forces on the cylinder is necessary. Few studies reported measurements that adhere to these requirements. Mohany and Ziada (2011) carried out dynamic lift measurements to analyze acoustic energy exchange mechanisms for a single cylinder, where the cylinder is supported on a stiff custom-design transducer to enable measurements of the fluctuating lift force. To investigate the excitation forces acting on stationary cylinders subjected to cross-flow at the coupling of vortex shedding and turbulence buffeting in water, Liu et al. (2017) carried out dynamic force measurements on normal triangular tube arrays.

The current understanding of flow instabilities that can excite acoustic resonance in inline tube arrays is still a subject of different theories. Early observations led to a view that there is no possibility for the development of coherent vortex shedding deep inside tube arrays due to the cumulative interactions with the tubes, and that any periodicity would be a result of random turbulence buffeting (Owen, 1965). The identification of persistent periodic flow phenomena deep within tube banks and the subsequent characterization of the Strouhal numbers by Chen (1984) refuted the earlier idea that no organized flow structures may form other than in the first few tubes of an array. A very careful and detailed investigation by Ziada and Oengoren led to the identification of up to three simultaneous periodic flow instabilities behind the first row of tubes in an inline tube array (Ziada and Oengören, 1992, 1993; Oengören and Ziada, 1998). Tests were carried out in air and water, leading to different flow characteristics depending on the fluid density, tube spacing, Reynolds number, and flow rate. Their results demonstrated that not all of these instabilities are capable of engaging in a feedback mechanism to cause acoustic resonance. The flow visualization carried out in water channels showed that a symmetric jet instability is responsible for organizing and syncing vortex shedding behind the first few rows of the inline tube array. An increase in the Reynolds number negatively impacted the number of rows with clear formation of vortices, while Ziada and Oengören (1992) argued that the feedback mechanism during acoustic resonance would result in synchronized vortex shedding behind multiple rows of the inline tube array due to the coupling of the stronger anti-symmetric jet instability with the acoustic field, which fundamentally contradicts the earlier understanding. However, the hypothesis that instabilities within gaps behind cylinders are responsible for the excitation of acoustic resonance in inline tube bundles was not fully confirmed until Mohany and Ziada (2005) reported it for the case of two tandem cylinders in cross-flow during pre-coincidence resonance. The simplified configuration of two tandem cylinders showed characteristics similar to inline tube bundles, and the study of the source of acoustic power pointed to the impingement of the flow instabilities in the gap between cylinders. Shaaban and Mohany (2019a) confirmed that an inline row of cylinders is capable of exciting pre-coincidence acoustic resonance. However, their results showed that the increase in acoustic resonance strength quickly diminished by increasing the number of inline cylinders and subsequently the number of gaps between them. Even at this simplified arrangement with only one inline row of cylinders, the achieved acoustic resonance was strikingly similar to that observed in a full inline tube bundle, which imposes a question about the effect of acoustic resonance on the flow structure. While previous reports provided some useful information about the conditions governing the occurrence of instabilities and their frequencies in inline arrangements of cylinders, flow visualizations were not carried out during resonance excitation, and extrapolations were not reliable. Therefore, there is a need to investigate the effect of pre-coincidence acoustic resonance excitation on the formation of coherent, clear vortices in the gaps behind successive cylinders. Moreover, investigation of the coupling mechanism and energy transfer between the flow field and the acoustic field by means of direct measurement of the dynamic lift forces acting on the cylinders can confirm, or refute, the uniformity of acoustic resonance excitation by all cylinders in an inline row.

At this point, a series of efforts have been carried out by the authors to clarify the underlying physics of the flow-sound interaction mechanisms in a set of interconnected flow configurations. First, the flow around a configuration of tandem cylinders provided a clear evidence that an important excitation mechanism could be hidden within the complex aeroacoustic response, and it is related to the phenomenon of interest in other flow configurations (Mohany and Ziada, 2005). Then experimental and numerical investigations of the excitation source in other configurations, particularly side-by-side cylinders and inline cylinders with uneven spacing, revealed other physical aspects of the resonance mechanism that never been reported before (Mohany et al., 2014; Arafa and Mohany, 2016; Shaaban and Mohany, 2019b). Recent data by the authors showed that accurate characterization of the interaction between multiple excitation mechanisms in *a relatively simple configuration* is important in order to develop adequate models that can be used to predict the excitation of acoustic resonance by flow around several related configurations (Shaaban and Mohany, 2019a). This interaction is not yet excavated in many configurations, including the case considered here for a set of inline cylinders.

To fulfill these research needs and provide the necessary tools for further development, this paper presents an investigation of the flow structure and the fluctuating lift forces acting on inline arrangements of cylinders during resonance excitation to identify the physical mechanisms that inhibit any significant increase in the acoustic resonance as the number of cylinders, and gaps, increases. The periodic cycle of flow field is measured at different phases of the acoustic cycle by means of phase-locked particle image velocimetry, and the flow structures are related to the excitation of the pre-coincidence acoustic resonance. Direct measurements of the dynamic lift forces are carried out for the configuration of multiple inline cylinders before the onset of acoustic resonance, as well as during pre-coincidence resonance, to quantify the added loading on the cylinders due to resonance excitation. The dynamic lift forces are then decomposed with respect to the resonant sound field to investigate the energy transfer mechanism and identify the contribution of the different individual cylinders in each configuration to the resonance excitation.

2. Experimental methodology

Measurements of acoustic pressure, particle image velocimetry, and dynamic lift force are carried out in an open-loop wind tunnel. The flow velocity is controlled through changing the rotational speed of a centrifugal blower, which allows achieving upstream flow velocities up to 150 m/s, equivalent to a Mach number of 0.43. Acoustic resonance excitation is often observed at Mach numbers below 0.35, giving no rise to significant compressibility effects. A detailed description of the wind tunnel is available in previous articles (Shaaban and Mohany, 2019a). A test section with a width

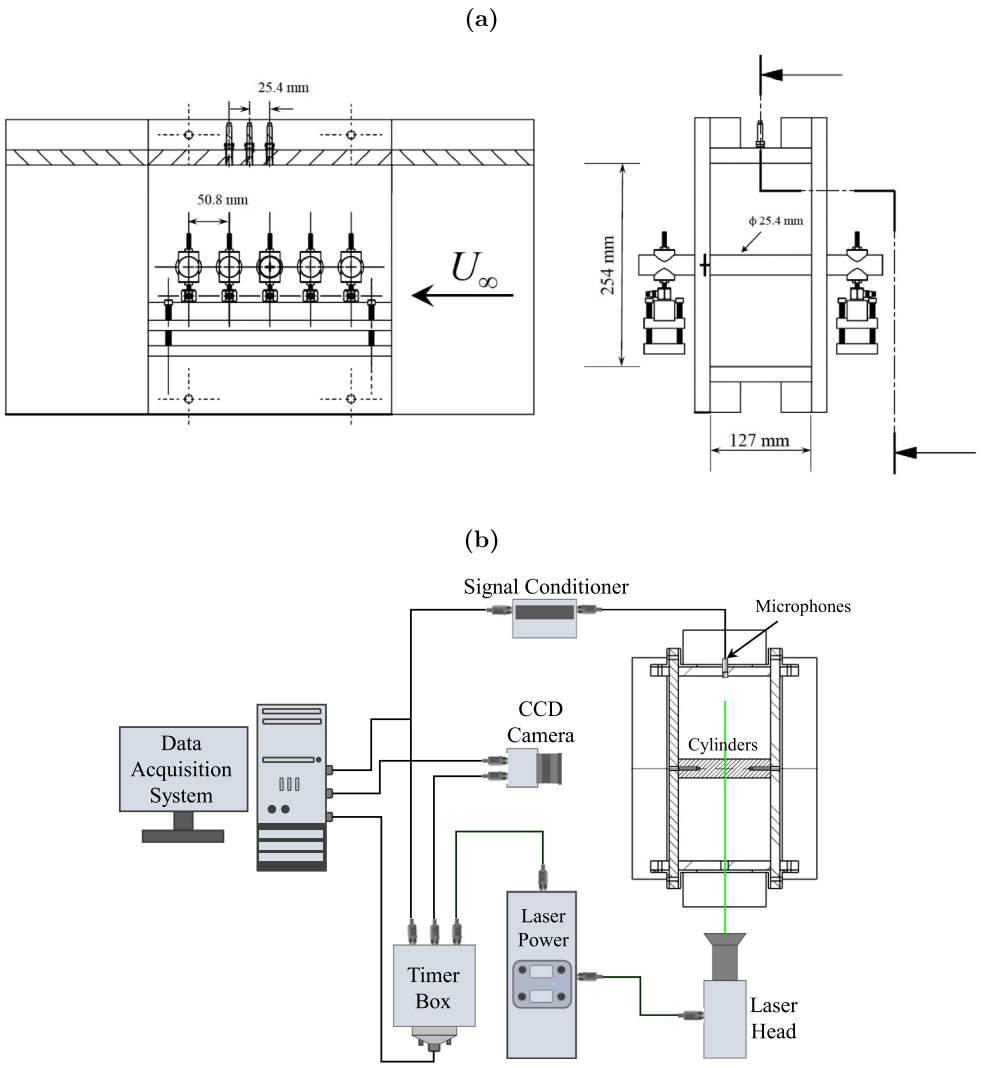


Fig. 1. (a) The test module and the setup for lift force measurements when five inline cylinders are installed and (b) A schematic of the particle image velocimetry setup.

$B = 127$ mm and a height $H = 254$ mm is used to carry out the experiments. At the necessary flow conditions, the acoustic characteristics and the dimensions of the rectangular test section allow for the excitation of the first acoustic cross-mode with acoustic pressure anti-nodal surfaces on the top and bottom walls, with an anti-nodal plane of acoustic velocity at the middle of the test section. The dimensions of the rectangular test section were selected to allow for self-excitation of pre-coincidence acoustic resonance at a flow velocity in the middle range of the maximum achievable in the wind tunnel. A row consisting of a number of inline cylinders ranging from two to five, with a diameter $D = 25.4$ mm is attached horizontally at a center-to-center spacing $L/D = 2.0$. Cylinders extend from side to side in the middle of the test module height, resulting in an area blockage of 10%, which is consistent throughout all investigated cases. To verify the uniformity of flow conditions along the span of the cylinder, measurements of the surface pressure on a single cylinder were carried out over Reynolds number between 1.3×10^4 and 6.4×10^4. The base pressure coefficient was measured using pressure taps along the span of the cylinder at 180° from the upstream stagnation point. These measurements showed that the base pressure coefficient is uniform within 4% of its mean value over 94% of the cylinder's span. Moreover, profiles of the pressure coefficient over the circumference of the cylinder at its mid-span and near the side walls agree well with the measurements of Norberg (2002). Hotwire measurements inside the test section, with no cylinders, indicated that the maximum turbulent intensity is less than 1 %. The design of the wind tunnel allows for a uniform upstream flow velocity within 95% of the test section height. In all tested cases, measurements and analysis were carried out for the first acoustic cross-mode of the test section, with acoustic particle velocity perpendicular to both the streamwise direction and the cylinder axis.

During each experimental run, the flow velocity inside the test section is measured using a Pitot tube installed at the middle point of the test section. When aeroacoustic signals are recorded, the Pitot tube is removed from the test section so that it does not excite any additional acoustic modes or create artificial flow structures that may interfere with the measured quantities. The acoustic pressure is measured using a PCB pressure microphone (model 377A12) with a diaphragm diameter of 6.35 mm and a nominal sensitivity of 25 mV/kPa flush-mounted at the top wall of the test section. The microphone signal is processed by a compatible pre-amplifier (PCB model 426B03), after which the signal is processed into a voltage output by an ICP signal conditioner (PCB model 482C15). The sensitivity of the microphone is calibrated using a piston phone (GRAS model 42AB). The microphone is firmly fixed using a teflon O-ring inside a metal fitting. Measurements using several microphones spaced by 1 inch in the streamwise directions showed that the acoustic pressure signals along this section of the top wall do not deviate significantly, and are exactly in phase during the excitation of an acoustic standing-wave of a resonant mode.

In order to investigate the effect of the number of inline cylinders on the periodic flow field during resonance, phase-locked PIV measurements were carried out at the mid plane of the test module as shown in Fig. 1b. A pulsed Nd:Yag laser with a wavelength of 532 nm enabled the capture of image pairs of the illuminated measurement plane. A CCD camera was used to capture images with a resolution of 2752 pixel$\times$2200 pixel. The air flow was seeded with particles of Bis(2-ethylhexyl) sebacate (DEHS), atomized using a Laskin nozzle generator to particles with a mean diameter of approximately 1 μm. PIV measurements for different cases were carried out at a flow velocity that corresponds to the maximum acoustic pressure amplitudes during resonance excitation. The acoustic pressure signal was used to trigger the PIV system to take pairs of images. To acquire the flow field at a certain phase angle with respect to the acoustic pressure, the laser pulses were set to occur at selected time delay(s) after the trigger by the acoustic pressure signal. Eight sets of measurements were taken at eight uniformly spaced phases of the acoustic cycle. For each phase, 250 instantaneous images were acquired. The time between pulses was adjusted to capture the maximum particle displacement within one-quarter of the final interrogation window used for vector calculation, which are performed using multi-pass cross-correlation algorithm with one pass at initial window size of 64 $\times$ 64 pixels with 50% overlap and four final passes at interrogation window size of 32 $\times$ 32 pixels with 50% overlap. The final vector field has a uniform spatial resolution of $0.06D \times 0.06D$ in the x and y coordinates. At these conditions, the average velocity field at each phase is evaluated with a maximum uncertainty of $\pm$3.1 m/s, or less than 4.0% of the incoming flow velocity U_∞.

In order to identify the differences in the excitation mechanism of multiple inline cylinders of equal diameters, measurements are carried out for two, three, four, and five inline cylinders. Measurements of fluctuating lift force on multiple inline cylinders are performed simultaneously with the acoustic pressure measurements at resonant and non-resonant conditions. Up to five individual force sensors (PCB model 208C01) with nominal sensitivity of 112 mV/N are used to measure the fluctuating lift force on the cylinders. Each sensor has a measurement range of $\pm$ 44.5 N, with a resolution of 45 μN. The sensor does not need additional external pre-loading as the installed external mounting hardware places the sensor in a pre-loaded state, allowing it to accurately measure dynamic lift force in both tension and compression state. The high stiffness of the sensor (1.05×10^9 N/m) enables measurements of forces at frequencies up to 36 kHz. The force sensors are installed on a specially designed mounting assembly on which the cylinders are supported. The cylinders cross the test section side windows through a gap of 1 mm. An oiled rubber O-ring is attached to the surface of each cylinder on the outer face of the side window to prevent any flow disruption in the test section, without affecting the force measurements. The force sensors are firmly installed using ANSI 10–32 screws that fit in threaded holes in the bottom surface of the sensor and the top of the mounting assembly. A similar thread is attached into the threaded hole on the upper side of the sensor to allow for cylinders installation. Each cylinder is firmly attached to the thread using two nylon saddle washers. A different pair of side windows with the right number of holes is used for each experiment. The sensors are mounted on a stiff steel bar on which the mounting threaded holes are drilled. The bar fits in a key channel on a steel leveling plate with four fine threads on the four sides to adjust the alignment of the inline cylinders. To characterize the phase response of the sensors, pluck tests were used to calculate the phase difference between the available sensors with respect to a reference sensor. At the frequency of acoustic resonance, around 670 Hz, all sensors had negligible phase difference.

The lift force assembly is installed on rigid supports that are firmly mounted on threads into the ground and isolated from the test section supports. The support structure consists of square steel beams welded together to provide high stiffness and to reduce any vibration interference with the force measurements. Measurements of the dynamic lift force carried out on the two sides of the cylinders showed that each of the two sides is affected by exactly half of the total dynamic lift fore. The sensors attached on the two sides also measure negligible phase difference, especially at resonant conditions, as discussed in the following section. In the experiments with four and five inline cylinders, the force sensors are attached at one side of the cylinders and the other side is attached on a rigid threaded support that is identical to the force sensor configuration to keep side-to-side support symmetry.

The temperature and humidity of air are controlled in the lab to be around 25° and 50% and are recorded using indoors climate sensors for each experiment. Before the start of each experiment, the motor is run for enough time in the room to reach steady temperature state. Starting each run, the flow velocity is increased gradually to the desired value by increasing the rotational speed of the motor. When the flow velocity reaches the required value and stays steady for one minute, measurements take place for another minute. The motor rotational speed is increased in steps of around 60 rpm, increasing the flow velocity around 2.5 m/s each step. At resonant conditions, the flow velocity is increased in smaller steps to capture details of the aeroacoustic response.

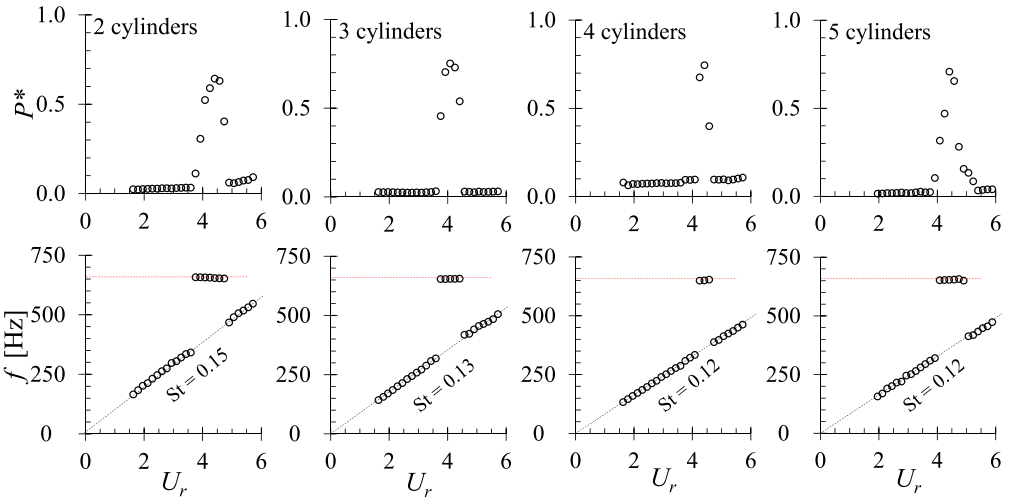


Fig. 2. The effect of reduced velocity on the normalized pressure and frequency representing the aeroacoustic response of the arrangements of two, three, four, and five inline cylinders with a center-to-center spacing ratio $L/D = 2.00$.

The acoustic pressure and force signals are recorded using a data acquisition system (NI model BNC-2110) at a sampling rate of 20,000 samples per second which is sufficiently higher than the Nyquist sampling rate, as the maximum expected frequency of interest does not exceed 2 kHz. The length of the recorded signal is 60 s, which is then blocked into 1 s samples. The ensemble average of the 60 samples is calculated with a Hanning window at 50% overlap to obtain the spectral characteristics of the signal. The resulting spectra have a resolution of 1 Hz, and the frequency at the peak acoustic pressure is manually detected. The acoustic pressure reported throughout this work is the root mean square of acoustic pressure signal after passing the signal on a high pass eighth degree filter that filters frequency content below 100 Hz. Likewise, a similar analysis procedure is used to calculate the fluctuating force coefficients. The phase between different samples is calculated as the angle of the complex transfer function between the two signals, calculated from the estimates of the power spectral density (PSD) using Welch's overlapped segment averaging estimator. Measurement of flow velocity U is accurate within $\pm 2.3\%$, and the acoustic pressure amplitude P_a is measured with an uncertainty of $\pm 0.9\%$. The amplitude of the dynamic lift coefficients on cylinders is reported with an uncertainty of $\pm 4.7\%$.

3. Periodic flow structures around a row of inline cylinders in presence of acoustic resonance

Fig. 2 represents the aeroacoustic response of the investigated configurations. The figure shows a reasonably similar response for all configurations in terms of the onset, progression, and decay of resonance, the peak normalized acoustic pressure, and the peak frequency f in the pressure spectra. The acoustic response of each arrangement is represented by the root mean square of the acoustic pressure at each flow velocity, where the flow velocity and the pressure are expressed in their normalized form U_r and P^*, defined as

$$U_r = \frac{U_\infty}{f_a D} \tag{1}$$

$$P^* = \frac{2P_{\text{rms}}}{\rho U_\infty^2} \tag{2}$$

where f_a is the acoustic mode frequency and P_{rms} is the root mean square acoustic pressure. For all four cases, the frequency jumps suddenly from around 300 Hz to a significantly higher value of 670 Hz, which is the first acoustic cross-mode frequency of the test section. The jump in frequency is associated with a surge in the normalized pressure from low levels that are characteristic of turbulent flow noise to values in the order of 0.75. The maximum normalized pressure increases slightly as the number of cylinders is increased from two to three. As the number of inline cylinders is further increased, the increase in the normalized pressure is within the margin of uncertainty. This observation is rather counter intuitive, as the pre-coincidence resonance is known to result from instabilities of the flow separating at one cylinder and impinging on the cylinder directly downstream. When more gaps exist, it would be expected that the acoustic resonance would have a stronger array of sources that would result in higher acoustic pressure. Instead, no significant increase in the normalized pressure could be achieved as the number of cylinders was increased beyond three. Previous investigations in the same test section showed that other configurations, such as tube bundles, finned cylinders, or inline cylinders of larger diameters may excite acoustic resonance of significantly higher amplitudes, which indicates that the acoustic mode in the test section has not reached a limit imposed by a "limit cycle" where acoustic energy dissipation would prevent

the generation of higher acoustic pressures. Therefore, the limited acoustic pressure is thought to be imposed by the features of the flow around the different configurations, and the mechanism by which the flow field transfers energy to the acoustic field during resonance excitation.

Fig. 3 shows the flow streamlines and contours of normalized vorticity $\omega D/U_\infty$ around the configuration of two tandem cylinders at a flow velocity $U_\infty = 71$ m/s, equivalent to $U_r = 4.3$. At this flow velocity, self-excited acoustic resonance resulted in a steady tone at a frequency of $f_a = 650$ Hz, with the maximum acoustic pressure $P_{\text{rms}} = 2.1$ kPa for this configuration. The figure shows the flow field at eight different phase angles ϕ_p of the acoustic pressure. During excitation of a resonant standing-wave cross-mode, the acoustic particle displacement d_a is temporally in-phase with the acoustic pressure. The acoustic particle velocity is therefore out-of-phase with the acoustic pressure by 90°. At the start of the acoustic cycle, the acoustic pressure p is rising from an instantaneous value of zero, and the acoustic particle velocity u_a is at its maximum value. At each phase angle, the relative amplitude and direction of the acoustic particle velocity u_a at its antinode, located at the middle of the test section, is represented by a vector of an arbitrary scale. Solid cylinders obstruct the laser sheet, resulting in absence of data in a region at the negative values of y and $x = x_{c,i}$ where $x_{c,i}$ are the coordinates of cylinder centers. This constraint, however, does not degrade the value of the data, as the main interest is the flow within the gaps between cylinders, where impingement of the shear layers is the main source of instability that couples with the acoustic field. Fig. 3 clearly shows the impingement of the separated shear layer on the downstream cylinder. A vortex core forms in the gap then impinges on the surface of the downstream cylinder, then the flow separation on the downstream cylinder leads to the formation of distinct alternating vortex cores that are then shed downstream. The separating shear layer from the downstream cylinder has weaker vorticity, but the acoustic resonance clearly leads to a consistent formation of organized flow structures downstream of the cylinders at a frequency of $f_a = 654$ Hz, which would not exist in absence of acoustic resonance at this flow velocity (Shaaban and Mohany, 2019b). A reasonable degree of symmetry is observed for the forming cores.

Fig. 3 also shows that the flow field follows the acoustic particle velocity vector in time. When the acoustic particle velocity u_a is maximum, the wake streamlines are displaced to their extreme y positions, compared to their positions when $u_a = 0$. The shear layers within the gap between the two tandem cylinders, as well as the wake downstream of the cylinders, are influenced by the acoustic field and flap in synchronization with each other and with the vector u_a, which shows that the acoustic field indeed plays a role in organizing the flow field.

Fig. 4 shows the normalized vorticity field and streamlines during acoustic resonance excitation by flow around three inline cylinders. The flow field is measured at $U_\infty = 73$ m/s, and results in resonance with a maximum acoustic pressure $P_{\text{rms}} = 2.2$ kPa, which is within the margin of error from the value observed for the case of the two cylinders. However, the presence of the most downstream cylinder had a definite effect on the flow field. The flow field exhibits interesting features regarding the phase with the acoustic cycle, and the periodic features around the cylinders. First, the separation and impingement around the middle cylinder, i.e. in both the first and the second gaps, are not significantly different in phase from the case of two cylinders shown in Fig. 3. The cycle starts with the shear layer about to impinge on the middle cylinder for both cases. Weaker vorticity is observed in the downstream gap due to the effect of the upstream flow and the feedback of the Rossiter mode from the downstream cylinder. Strong vortex flow is evident only in the first gap, while the downstream gap shows separation and impingement. Most importantly, the vortex cores shed from the middle cylinder are smaller and weaker. Upon interaction with the most downstream cylinder, larger but more distorted cores are observed downstream of the configuration of three inline cylinders. Streamlines shown in Fig. 4 suggest that gap flow is possible, which would disrupt the impingement process, reducing the effectiveness of the acoustic energy production mechanism. While not significantly affecting the vorticity strength around the upstream and middle cylinders, the self-excitation of resonance by the flow field leads to steady formation of vortex cores, but interactions with the downstream cylinder leaves these cores more distorted, potentially affecting the exchange of energy around the most downstream cylinder.

An additional incremental degradation can be seen in Fig. 5 which shows the vorticity field and the streamlines for an acoustic cycle for the configuration of four inline cylinders. The flow cycle is still periodic as expected due to the lock-in with the steady tonal acoustic resonance. However, vortex interaction with the additional cylinder injects more distortion around that cylinder. The vortex cores around the third and downstream cylinders are fragmented, and tend to flow away from the cylinders. The flow velocity for this configuration is $U_\infty = 76$ m/s, and the maximum acoustic pressure stays at $P_{\text{rms}} = 2.3$ kPa. The modest increase in acoustic pressure stems from the slight increase in the flow velocity at the peak resonance level.

The coherent periodic structures around the two upstream cylinders suggest that resonant sound source will be localized around those two cylinders, while the interactions around the downstream cylinders would have less contribution to the excitation of resonance. However, the periodicity of the flow structures still shows alternating, though highly distorted shedding around the two most downstream cylinders. Streamlines show that strong vortex flow is only observed within the upstream gap, and that the other two gaps generally follow the direction of the acoustic particle velocity vector u_a. The gap between cylinders 2 and 3 also features gap flow, and impingement of the shear layer on cylinder 3 would not be persistent.

Characteristics of the flow cycle shown in Fig. 6 assert the same trend. The vorticity field and vortex cores around five inline cylinders are shown at an upstream flow velocity of $U_\infty = 80$ m/s during self-excitation of acoustic resonance with $P_{\text{rms}} = 2.4$ kPa. The first two gaps exhibit visible distinct cores that later interact with the remaining downstream

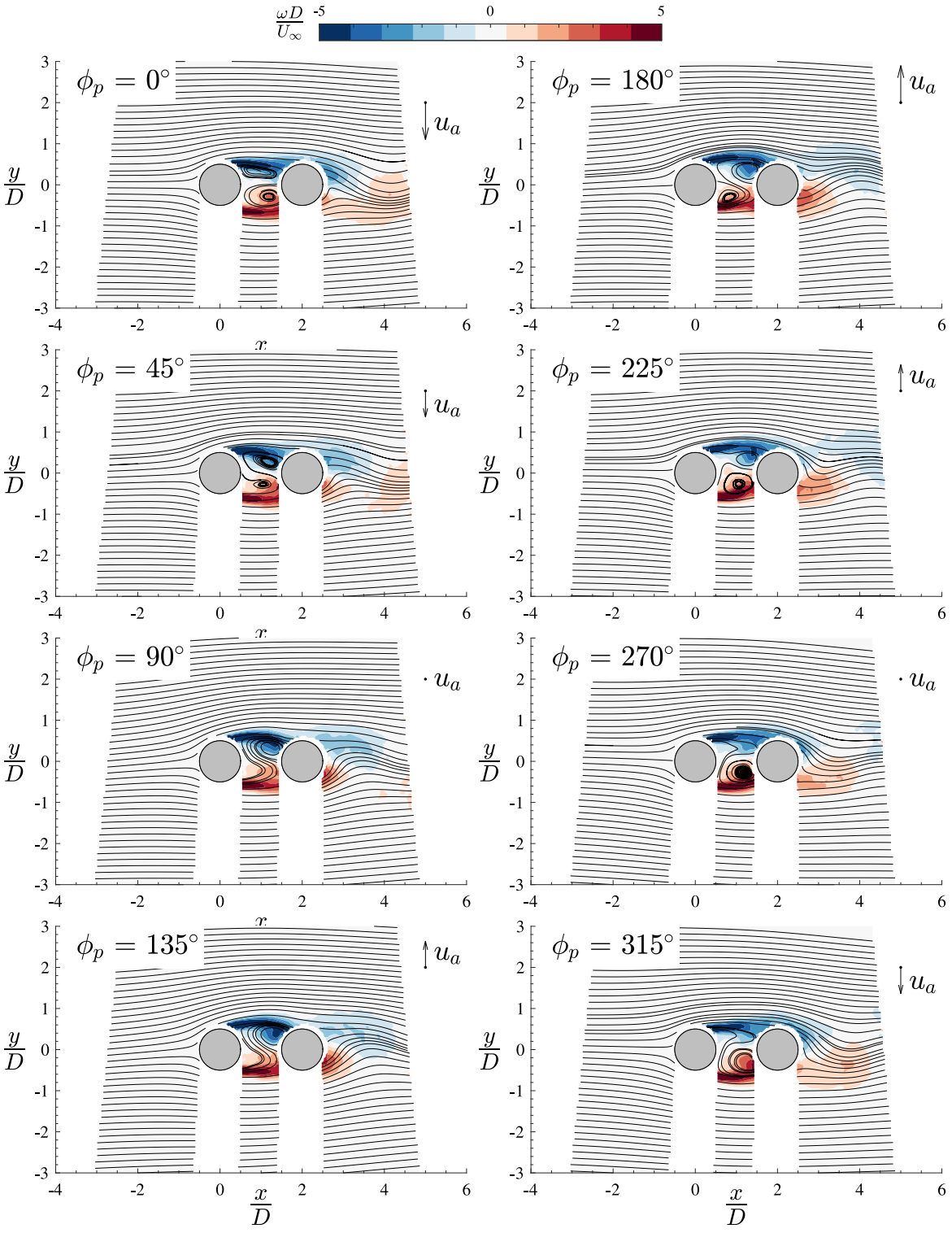


Fig. 3. The vorticity field and streamlines around two tandem cylinders over an acoustic cycle.

cylinders of the row and start to distort and become more fragmented. Weaker vorticity can be seen in the two most downstream gaps, possibly due to the effect of the upstream cylinders on the mean flow velocity around these cylinders.

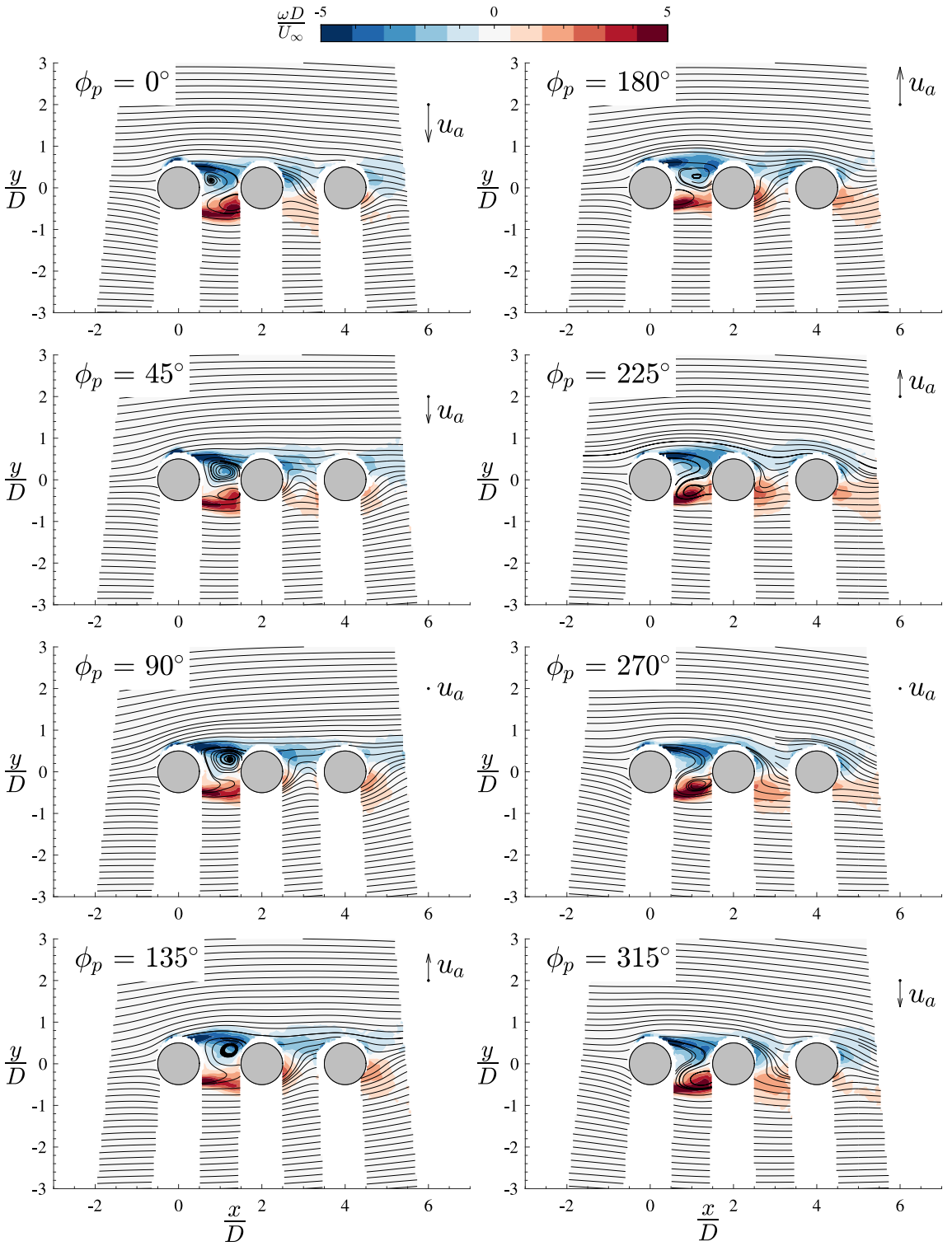


Fig. 4. The vorticity field and streamlines around three inline cylinders over an acoustic cycle.

As a result, alternating vortices are shed around the row, albeit being weaker and fragmented. Streamlines also show that gap flow is evident in some of the gaps, notably the gap between cylinders 3 and 4, which is expected to affect how these cylinders interact with the acoustic field. This trend is expected to continue as more cylinders are added. It

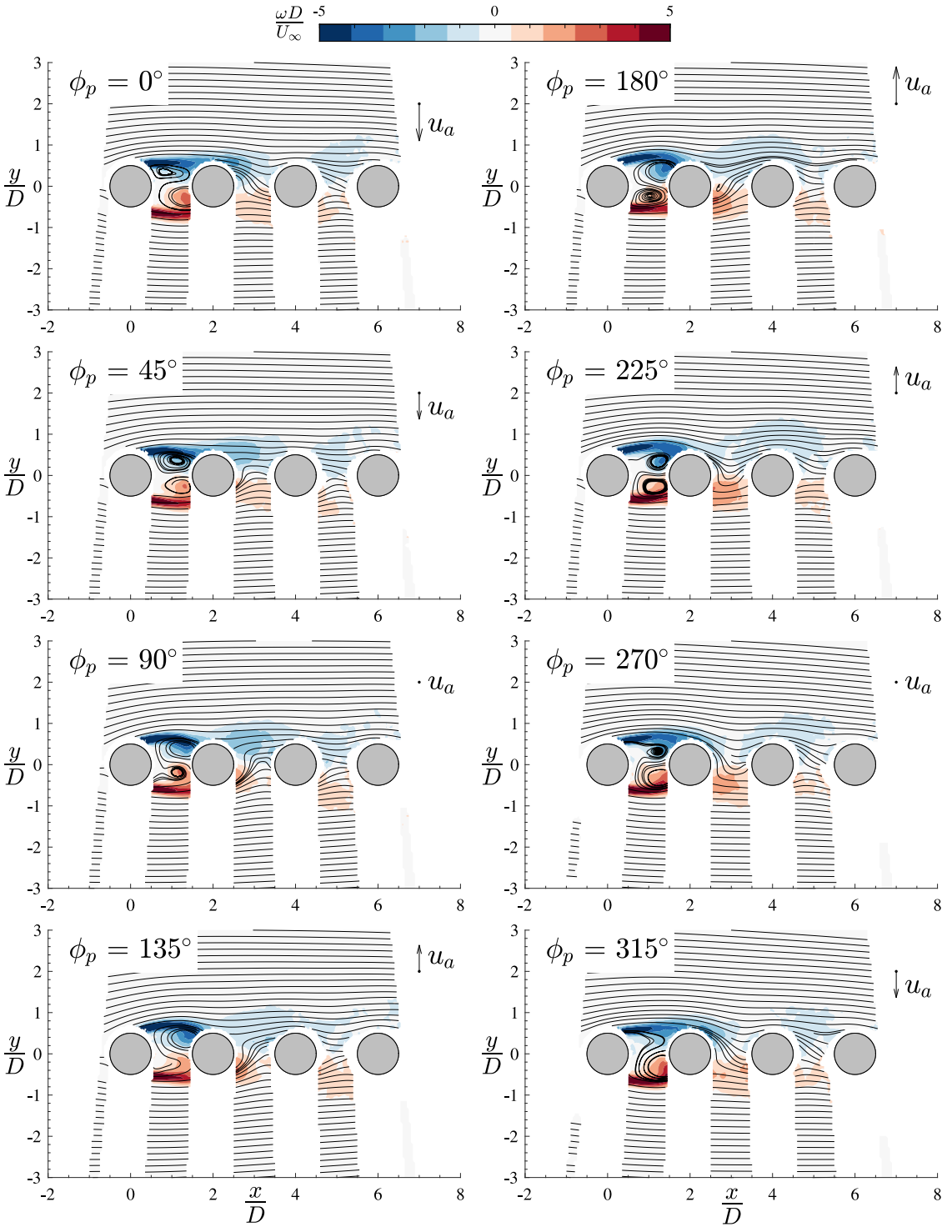


Fig. 5. The vorticity field and streamlines around four inline cylinders over an acoustic cycle.

can also be reasonably expected that if the row is surrounded by other rows such as the case of inline tube bundle with typical transverse spacing, more flow-structure interactions would make this distortion more pronounced. In this case, a turbulent jet flow would dominate the flow within the channels after the first few rows. This flow field potentially has

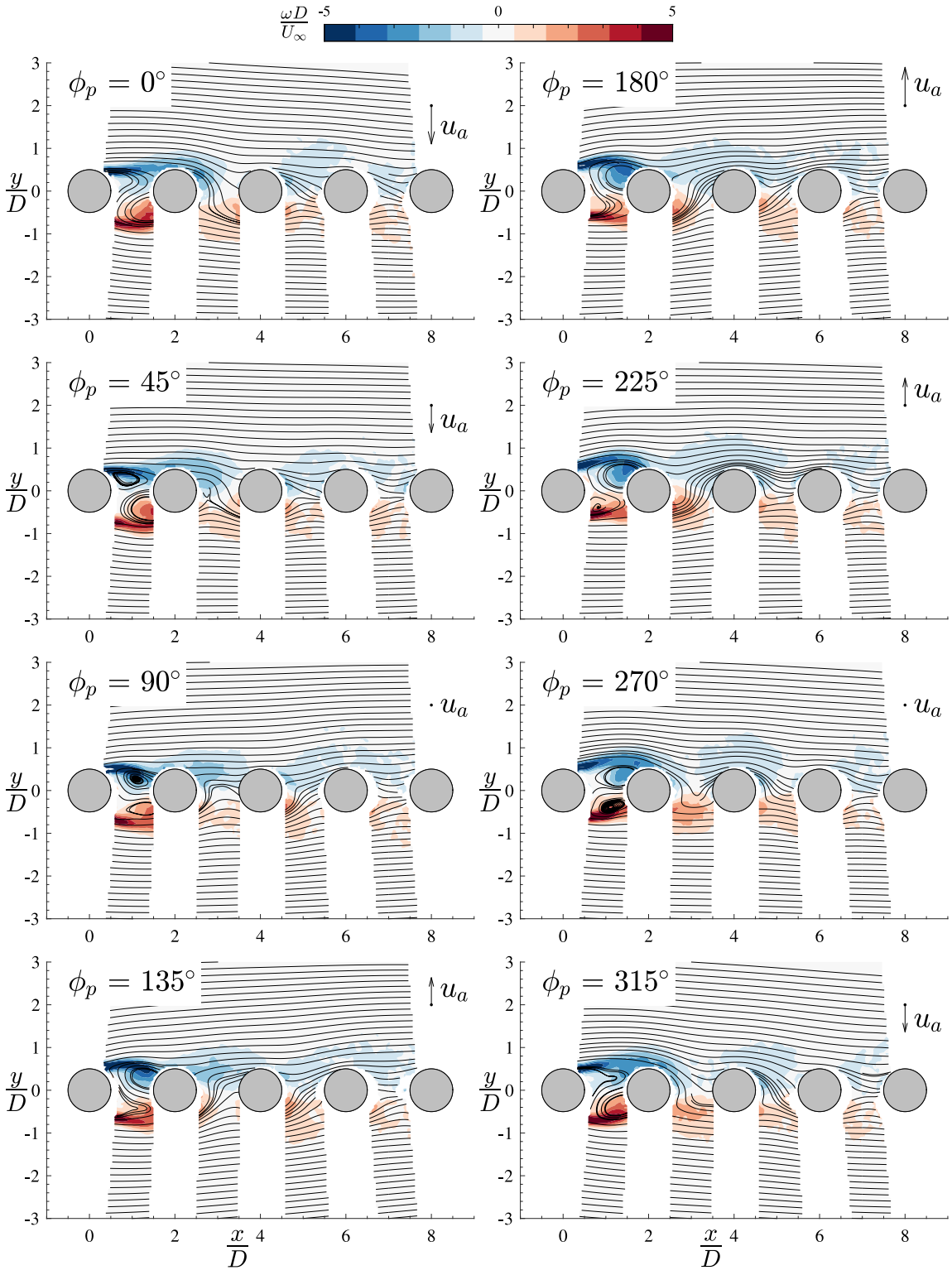


Fig. 6. The vorticity field and streamlines around five inline cylinders over an acoustic cycle.

major consequences on the location of the sound source(s) and on the coupling mechanism between the sound and flow fields, as will be reviewed in the following discussion.

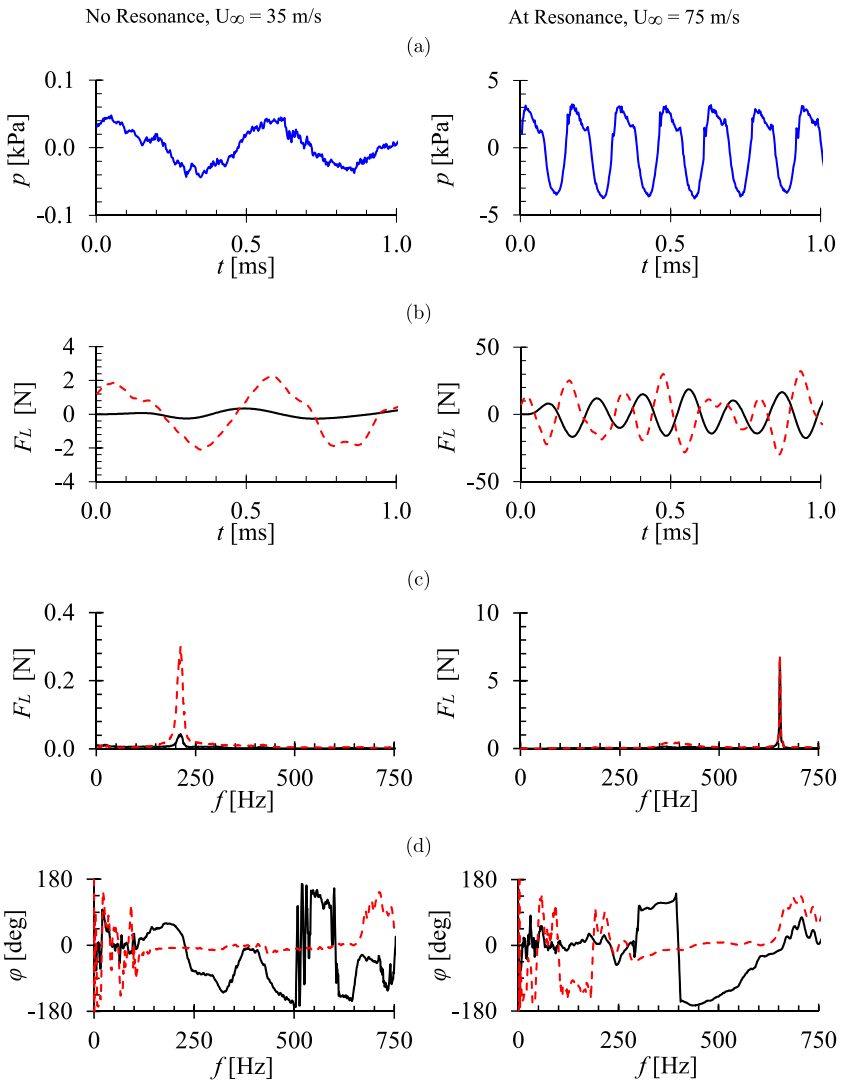


Fig. 7. Effect of resonance excitation by two tandem cylinders on (a) the acoustic pressure signal, (b) the lift force time signal, (c) the spectra of the lift force (d), and the phase of lift force with respect to the acoustic pressure. —— Upstream cylinder, - - - Downstream cylinder.

4. Effect of acoustic resonance excitation on dynamic lift forces on a row of inline cylinders

Fig. 7 shows the effect of the resonance excitation on the measured quantities for the case of two tandem cylinders. The data is shown for a flow velocity $U_\infty = 35$ m/s, which does not result in self-excitation of acoustic resonance, and a flow velocity $U_\infty = 75$ m/s at which the pre-coincidence resonance is self-excited. In the left column of Fig. 7, a sample measurement at $U_\infty = 35$ m/s is presented, showing the dynamic lift force F_L as well as the acoustic pressure over a time of 10^{-3} s. At $U_\infty = 35$ m/s, the acoustic pressure shows periodic fluctuations within $\pm$ 50 Pa. The dynamic lift force on the upstream cylinder is significantly lower, with a root mean square value not exceeding 0.05 N. The downstream cylinder is affected by significantly higher forces reaching $\pm$ 2.0 N. The dynamic lift force on the downstream cylinder is nearly in phase with the acoustic pressure, while the dynamic lift coefficient on the upstream cylinder leads both signals at the dominant frequency. In the frequency domain shown in Fig. 7c, the dominant component for the three signals is at the same frequency, at a Strouhal number of $St = 0.15$, which is typical for the wake shedding of two tandem cylinders at a spacing ratio of $L/D = 2.00$ in this range of Reynolds number.

Fig. 7d shows the phase φ between the dynamic lift force and the acoustic pressure. The figure shows that the lift force on the downstream cylinder had a steady phase with the acoustic field over a wide range of frequencies at this flow velocity. In the following discussions, the value of the phase between lift force and acoustic pressure is taken at the dominant frequency of fluctuations that is determined from the spectral analysis, as in Fig. 7b. Measurements showed that

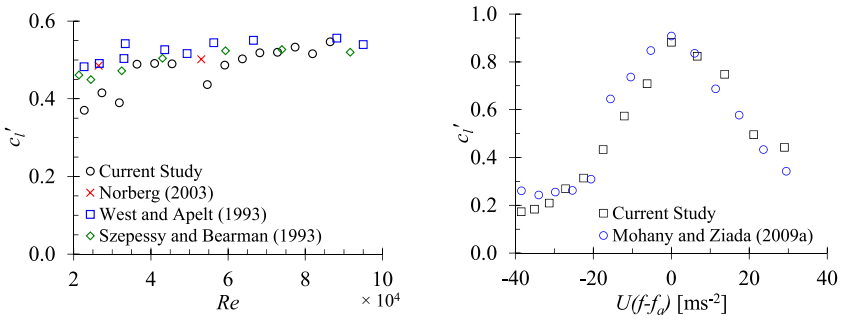


Fig. 8. Validation of the experimental measurements **(a)** dynamic lift force on a single cylinder over a range of Reynolds numbers, **(b)** dynamic lift force amplitude during excitation of acoustic resonance. (See Norberg, 2003; West and Apelt, 1993, 1997; Szepessy and Bearman, 1993; Mohany and Ziada, 2009a).

the dynamic lift forces on the two sides of the cylinder are nearly equal and in phase, which means there is no dynamic moment component on the cylinder.

The plots at the right column of Fig. 7 show a sample measurement at a flow velocity $U_\infty = 75$ m/s. In contrast with the previous case, the acoustic pressure and the lift force are significantly higher. In this self-excited resonance condition, high pressure fluctuations are detected at the antinode of the acoustic cross-mode, where the instantaneous acoustic pressure reaches nearly $P_a = \pm$ 4000 Pa. Fig. 7c shows an acute tone for the three signals at the acoustic cross-mode frequency $f_a = 653$ Hz. At the dominant tone frequency, Fig. 7d shows that the phase between the acoustic pressure and the dynamic lift coefficient on each of the two cylinders at the dominant frequency is nearly the same.

In order to validate the experimental results, Fig. 8a compares the dynamic lift coefficient on a single cylinder with data in literature for the same range of Reynolds number. The current measurements agree well with data from other investigations and the overall increasing trend of the dynamic lift coefficient on the cylinder is also well captured at the same range of Reynolds number.

To validate the measurements of dynamic lift performed during self-excitation of resonance, Fig. 8b shows the dynamic lift coefficient c_l' for a single cylinder in a duct, compared with the results of Mohany and Ziada (2011). The diameter of the cylinder in the current study is $D = 25.4$ mm, larger than the case of Mohany and Ziada (2011) who used a smaller diameter $D = 15.8$ mm. The different diameters of the two compared cases shown in Fig. 8 cause the reduced velocity values to fall at different ranges of Reynolds number. To take the effect of the different diameters at the same acoustic mode frequency on the excitation conditions, dynamic lift coefficients for the two experimental sets are plotted against $U(f - f_a)$, which is equivalent to $U_r.D(f/f_a - 1)$. The value of $U(f - f_a)$ becomes zero at the condition for the maximum acoustic pressure amplitude. Fig. 8 shows a reasonable agreement with the results of Mohany and Ziada (2009a) over the range of acoustic resonance excitation, where the dynamic lift coefficients on the two cylinders surge to nearly the same levels.

In the presence of a dominant tone with a frequency f_v, the generated acoustic pressure can be expressed by Eq. (3).

$$p(t) = P_{\max} \sin(2\pi f_v t) \tag{3}$$

For arrangements of inline cylinders, the fluctuating lift force has significantly higher amplitude than the fluctuating component of the drag force (Arie et al., 1983). The force exerted by the solid surface of a cylinder can be therefore quantified by measurement of the time-dependent lift force. For rigid cylinders, the dynamic lift force per unit length can be assumed to be sinusoidal at the same frequency, as defined in Eq. (4).

$$F_L(t) = \frac{\rho U_\infty^2}{2} c_l' \sin(2\pi f_v t + \varphi) \tag{4}$$

where c_l' is the dynamic lift coefficient, and φ is the angle by which the dynamic lift force leads the acoustic pressure. Fig. 9 shows the measurement results for the cases of two, three, four, and five inline cylinders over a range of reduced flow velocities between 4.0 and 6.0. For the four different cases, the excitation of acoustic resonance was observed for a range of flow velocities much lower than needed for frequency coincidence, characteristic of the pre-coincidence resonance excitation mechanism, reported for cases of inline cylinder arrangements. In the first row of Fig. 9, measurements of the dynamic lift coefficients, c_l' on the upstream and downstream cylinders in a row of two tandem cylinders are shown. Cylinder 1, the upstream cylinder, is initially subjected to low dynamic lift coefficient of around 0.05, while the dynamic lift coefficient on cylinder 2, the downstream cylinder, is higher at a value of around 0.5, which agrees with the values reported by Arie et al. (1983) and Alam et al. (2003). At the onset of self-excited acoustic resonance, a significant increase in the lift coefficient on both cylinders is observed. At the peak of resonance, at a reduced velocity of $U_r = 4.5$, the lift coefficient on cylinder 1 increases an order of magnitude to 0.8, while the dynamic lift coefficient on cylinder 2 reaches 1.2. When the flow velocity is further increased, the end of the lock-in state is associated with a decrease in the dynamic lift

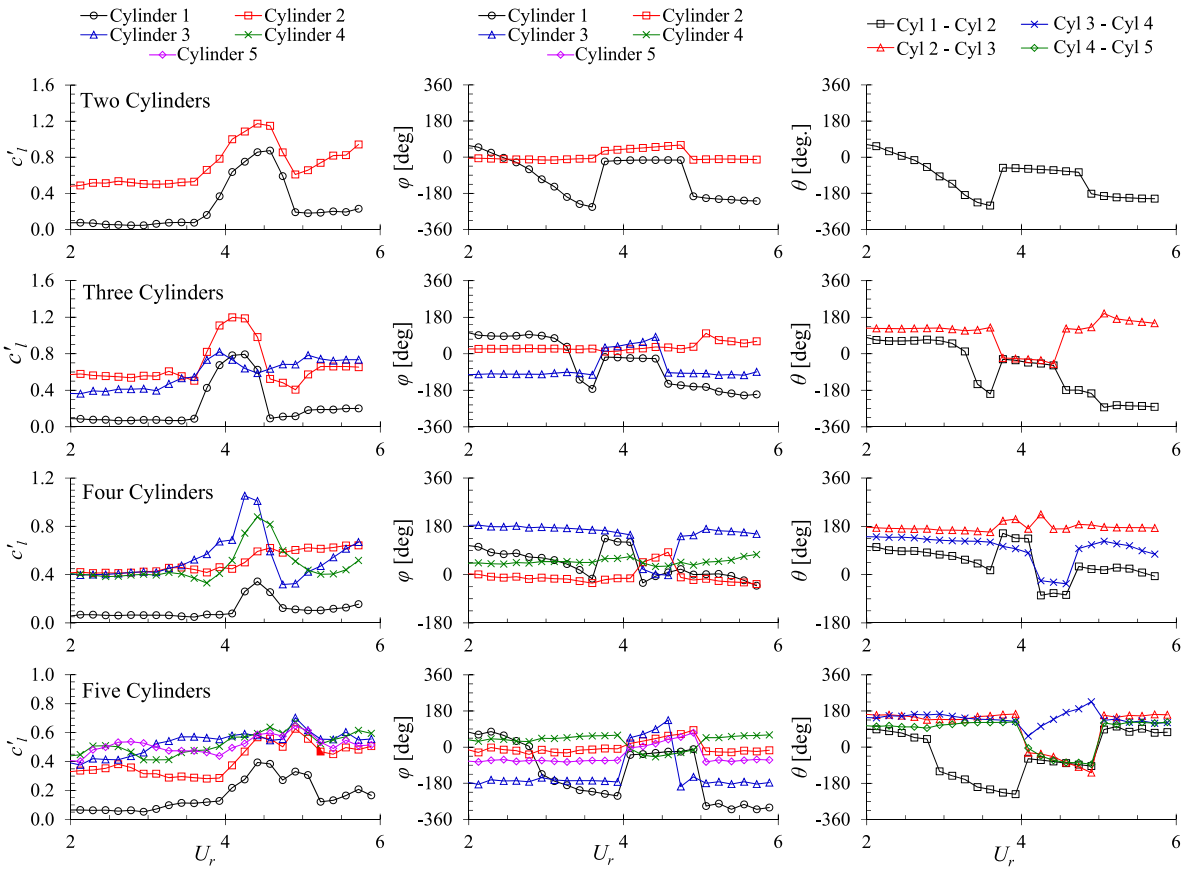


Fig. 9. The dynamic lift coefficient c_l', the phase of lift force and acoustic pressure φ and the phase between lift force on successive cylinders θ for configurations of inline cylinders $D = 25.4$ mm and $L/D = 2.00$ at a range of reduced velocities.

coefficients on both cylinders. At a reduced velocity of $U_r = 6.00$, the lift coefficients are slightly higher than their values before resonance, which is due to the significantly higher Reynolds number. The phase angle φ by which the dynamic lift on each cylinder leads the acoustic pressure at the dominant frequency, as per Eq. (4), is shown in the second column of Fig. 9. Initially, the dynamic lift coefficient on the downstream cylinder is in phase with the acoustic pressure. On the other hand, the phase angle between the dynamic lift coefficient on the upstream cylinder decreases from leading the acoustic pressure by 90° to lagging by 270°, which indicates that the acoustic pressure measured is produced by the vortex street shed at the wake of the downstream cylinder. At this range of flow velocities, the dynamic pressure of the vortex shedding acts as a dipole sound source that produces a traveling wave which then propagates to the surrounding area at the speed of sound. Outside the lock-in region, the microphone picks up the resulting dynamic signal of acoustic pressure with a negligible delay. The phase with the downstream cylinder therefore stays the same over this range of flow velocities. In contrast, the lift force on the upstream cylinder is determined by the flow in the gap between the two cylinders, which depends on Reynolds number. At the onset of resonance, the values of the phase angle φ increases abruptly, which indicates that the standing acoustic wave of the first acoustic cross-mode has a significant influence on the flow field, which is in turn reflected on the phase of the dynamic lift force. The dynamic lift force on the upstream cylinder becomes in phase with the acoustic field, while the dynamic lift force on the downstream cylinder has a positive phase angle φ with the acoustic pressure, showing that energy transfer is likely to occur between the flow and sound fields.

The phase angle between the dynamic lift on each two successive cylinders, $\theta = \varphi_i - \varphi_{i-1}$ is shown in the third column of Fig. 9, which has a close relationship to the flow field discussed in Figs. 3–6. Before the onset of pre-coincidence resonance, the dynamic lift on the upstream cylinder leads that on the downstream cylinder by nearly 90°. As the reduced velocity increases, the phase angle decreases gradually. At $U_r = 2.2$, the two dynamic forces are nearly in phase. Increasing U_r from 2.2 and until the onset of the pre-coincidence resonance at $U_r = 3.8$, the angle θ becomes increasingly negative. The pre-coincidence resonance causes a sudden jump of the phase angle as the dynamic forces on the two cylinders come nearly in-phase, indicating a change in the flow regime in the gap between the two cylinders induced by the acoustic resonance.

The second row of Fig. 9 shows the dynamic lift coefficients on the three cylinders. The dynamic lift coefficients on the three cylinders before the onset of resonance are 0.08, 0.58, and 0.36 for cylinders 1, 2, and 3, respectively. The lock-in region of the pre-coincidence resonance lasts over a range of reduced velocities between $U_r = 3.8$ to 4.6. The excitation of resonance causes an increase of the dynamic lift coefficients to 0.79, 1.18, 0.63 on cylinders 1, 2, and 3, respectively. After the lock-in condition ends, dynamic lift coefficients come back to their values before resonance. For the same arrangement of three inline cylinders, the value of the phase for cylinder 1 jumps between $U_r = 3.0$ and 3.5, prior to resonance, indicating a change in the flow regime around cylinder 1. The dynamic lift forces on cylinders 2 and 3 do not show noticeable phase change up to the onset of pre-coincidence resonance. The onset of resonance causes phase angles to jump closer in-phase with the acoustic pressure. During pre-coincidence, the dynamic lift on cylinder 3 leads the acoustic pressure. On the other hand, the dynamic lift on cylinder 1 is at a slightly negative phase angle with the acoustic pressure, suggesting that a significant component of the lift force on cylinder 1 is mainly sound-induced. The phase difference between the dynamic lift forces on Cylinder 2 and 3 and the acoustic pressure is positive, suggesting that the resonant field is driven by the flow structures interacting with these cylinders. Once the lock-in is over, the phase angles φ shifts back close to their original values. The phase shift between dynamic lift on cylinder 1 and cylinder 2 before resonance is around 80°, while the value is around 120° between dynamic lift on cylinder 2 and cylinder 3. Interestingly, the values of θ become equal at the onset of resonance. As the phase angle θ is related to the integrated flow structure between the two cylinders, this behavior indicates that the strong acoustic pressure oscillations influence the flow in the two gaps between the cylinders significantly. The nearly equal value of θ suggests that the flow structures in the gaps between cylinders operate in sync during resonance, resulting in the same phase of the lift force on each downstream cylinder for each gap. Such flow behavior plays part in the increase of P^* as the number of cylinders was increased from two to three.

The third row of plots in Fig. 9 shows measurements related to the dynamic lift coefficient on four inline cylinders over the measurement range. The dynamic lift coefficient on the upstream cylinder is significantly lower than its value on the three other cylinders. Before the onset of pre-coincidence resonance, cylinders 2, 3, and 4 are subjected to similar values of dynamic lift coefficients at the dominant frequency. The dynamic lift coefficients on the four cylinders diverge to different values during excitation of the pre-coincidence resonance. At the peak of the acoustic resonance, cylinder 3 is subjected to the highest dynamic lift coefficient, which reaches $c_l' = 1.1$. The dynamic lift coefficient on cylinder 2 increases slightly. At higher reduced velocities at which the lock-in condition ceases to exist, the values of the dynamic lift on the four cylinders revert back to their values before onset of resonance. During lock-in, the values of φ for all cylinders become close to each other, within the range of 0° to 90°, indicating that the strong acoustic oscillations affect the flow structures around the four cylinders. For the case of four inline cylinders, the phase angle θ between the dynamic lift on each pair of successive cylinders shows distinctive features that are not seen for the two cases already discussed. The flow structures in the gaps are evidently different during pre-coincidence resonance. For the lock-in region, dynamic lift forces on cylinders 1 and 2 are separated by $\theta = -70°$. Moreover, cylinders 3 and 4, surrounding the most downstream gap, are subjected to dynamic lift forces separated by θ around -30°. On the other hand, cylinders 2 and 3 are different in phase by a positive angle $\theta = 180°$. The upstream cylinder is subjected to a stagnation flow upstream and the initial wake separation, while the successive cylinders may be subjected to different flow structures depending on the flow regimes within each gap. This shows that although the acoustic pressure is strong enough to sustain the feed-back cycle and keep a lock-in condition, the flow regimes within the configuration can still have different characteristics, and are not necessarily fully organized by the strong pressure oscillations.

The fourth row of plots in Fig. 9 presents the dynamic lift coefficients on five inline cylinders, which show a rather complex progress with the reduced velocity indicating that the flow regimes feature an increasing number of interacting phenomena. Off resonance, the upstream cylinder is subjected to a significantly low dynamic lift coefficient, which is the case for the upstream cylinder in all other configurations. Cylinder 2 is subjected to a higher dynamic lift coefficient that ranged between 0.30 and 0.38 for a reduced velocity range up to $U_r = 4.0$. The dynamic lift coefficients on cylinders 3, 4, and 5 are higher than that on the two upstream cylinders, and change significantly depending on the reduced velocity, which shows a strong dependence of the flow regimes on the Reynolds number in absence of a resonant acoustic field. During pre-coincidence acoustic resonance, the dynamic lift coefficient on the five cylinders increased significantly and cylinders 2, 3, 4, and 5 were subjected to nearly the same dynamic lift coefficients, with high values that peaked to 0.63 at $U_r = 5.0$. After the lock-in condition of the pre-coincidence resonance ceases to exist, the values of dynamic lift coefficients decreased to the values observed before onset of resonance. Despite the complexity of the dynamic lift coefficient amplitudes, the phase angle φ has a traceable trend with the acoustic field. Similar to all previous cases, the increase in reduced velocity resulted in a gradual change of the phase of the dynamic lift coefficient on the upstream cylinder from leading to lagging the dynamic lift on all other cylinders. Dynamic lift on all other cylinders had a steady phase with the acoustic field that retained its value before and after the onset of pre-coincidence resonance. During lock-in, the dynamic phases jumped as the flow field started to exchange much more energy with the acoustic field through the feedback mechanism. As in all previous cases, lock-in condition brought dynamic lift coefficients on all cylinders closer in-phase with the acoustic pressure during resonance. The phase angle θ between dynamic lift coefficients on each two successive cylinders in the arrangement of five inline cylinders follows the behavior seen previously for four inline cylinders. The phase difference θ during lock-in is similar for three of the four pairs of cylinders. The three pairs, namely cylinder 1 with cylinder 2, cylinder2 with cylinder 3, and cylinder 4 with cylinder 5 have a value of θ around $-90°$. The

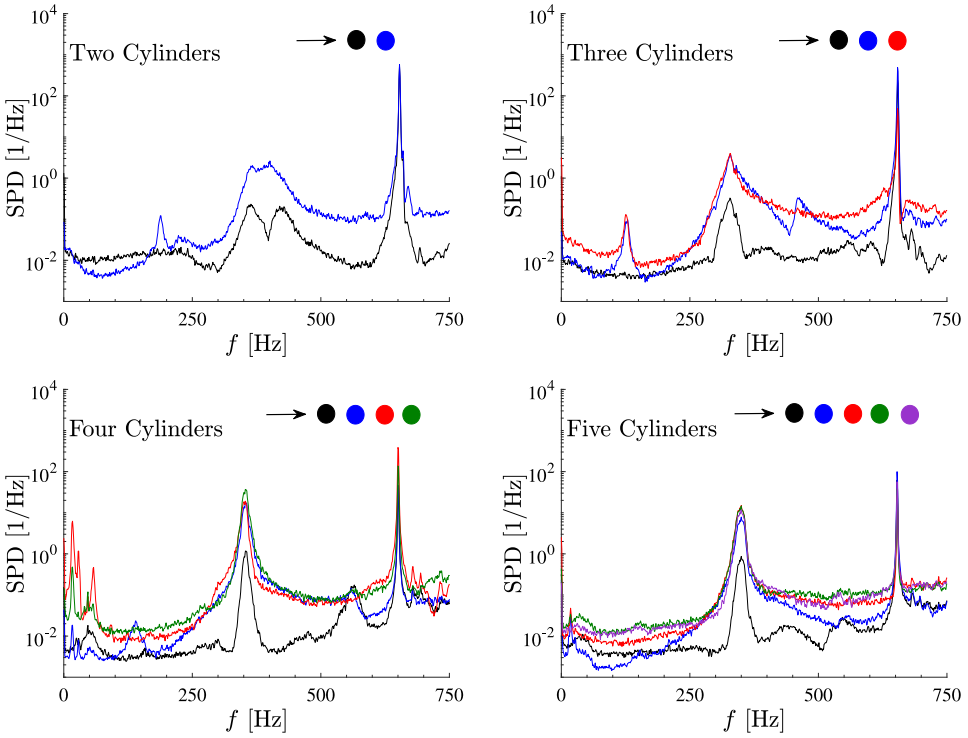


Fig. 10. Power spectral density of the fluctuating lift coefficient on cylinders in arrangements of two, three, four, and five inline cylinders at the peak of acoustic resonance excitation.

phase shift between dynamic lift on cylinders 3 and 4 is positive, and increases significantly during lock-in. This variation in the value of θ indicates that the strong acoustic oscillations during lock-in do not completely organize the flow regime within some of the gaps, which remains strongly dependent on the increasing value of Reynolds number.

It is important to relate the characteristics of the lift force observed in Fig. 9 to the characteristics of its coupled flow field shown in Figs. 3–6. The flow field was shown for cases during excitation of resonance. The synchronized structures evident in the flow field can explain the convergence of the phase angle φ to closer values during resonance. The lift force on the cylinders are a result of the synchronized shedding of the periodic structures, which occurred at the same frequency as the acoustic mode frequency. Away from resonance, it is therefore expected that completely different patterns of vortex formation and shedding prevail. The synchronized vortex patterns shown in Figs. 3–6, however distorted and fragmented, and the accompanying characteristics of the dynamic lift force shown in Fig. 9 are therefore closely related to the mechanism of resonance excitation, and any countermeasure aimed at controlling resonance excitation should primarily target these particular features.

Fig. 10 shows the energy power spectrum of the lift force signals on individual cylinders in each configuration during the self-excitation of acoustic resonance at its maximum level P_{rms}. For all configurations, sharp tonal excitation at the frequency of resonance f_a suggests that the flow field is oscillating strongly because of the coupled state. In addition, all cylinders also exhibit excitation at a frequency close to 350 hz, corresponding to a Strouhal number of 0.15. This value is related to the vortex shedding frequency developing around the row at a lower frequency than the shear layer separation and impingement, which during resonance is locked-in to a frequency equal to the acoustic cross-mode frequency. The vortex shedding peak, however, is orders of magnitude weaker than the acoustic resonance peak. That excitation, which does not participate in the pre-coincidence resonance excitation, is weakest on the upstream cylinder, and starts to become stronger on the rest of the cylinders. The frequency of this component is not at an integer fraction of the acoustic pressure cycle frequency, and therefore their interaction would lead to an increasing distortion of the periodic excitation around downstream cylinders, similar to that observed in Figs. 3–6. It is evident that while acoustic resonance made the acoustic mode frequency dominant, it did not completely mute the effects of the periodic vortex shedding component, leading to a lower efficiency of the acoustic resonance excitation mechanisms in the gaps between the downstream cylinders.

At the peak acoustic pressure amplitude, Fig. 11 shows the phase diagrams of the lift force on each cylinder for all arrangements with the acoustic pressure as a reference. The data in Fig. 11 is plotted using samples of 20 ms, with the data filtered using a fourth degree band-pass filter of limits $f_a \pm 100$ [Hz]. As any noise with frequencies away from the acoustic mode frequency f_a was filtered out, the phase between the lift force and the acoustic pressure results in a

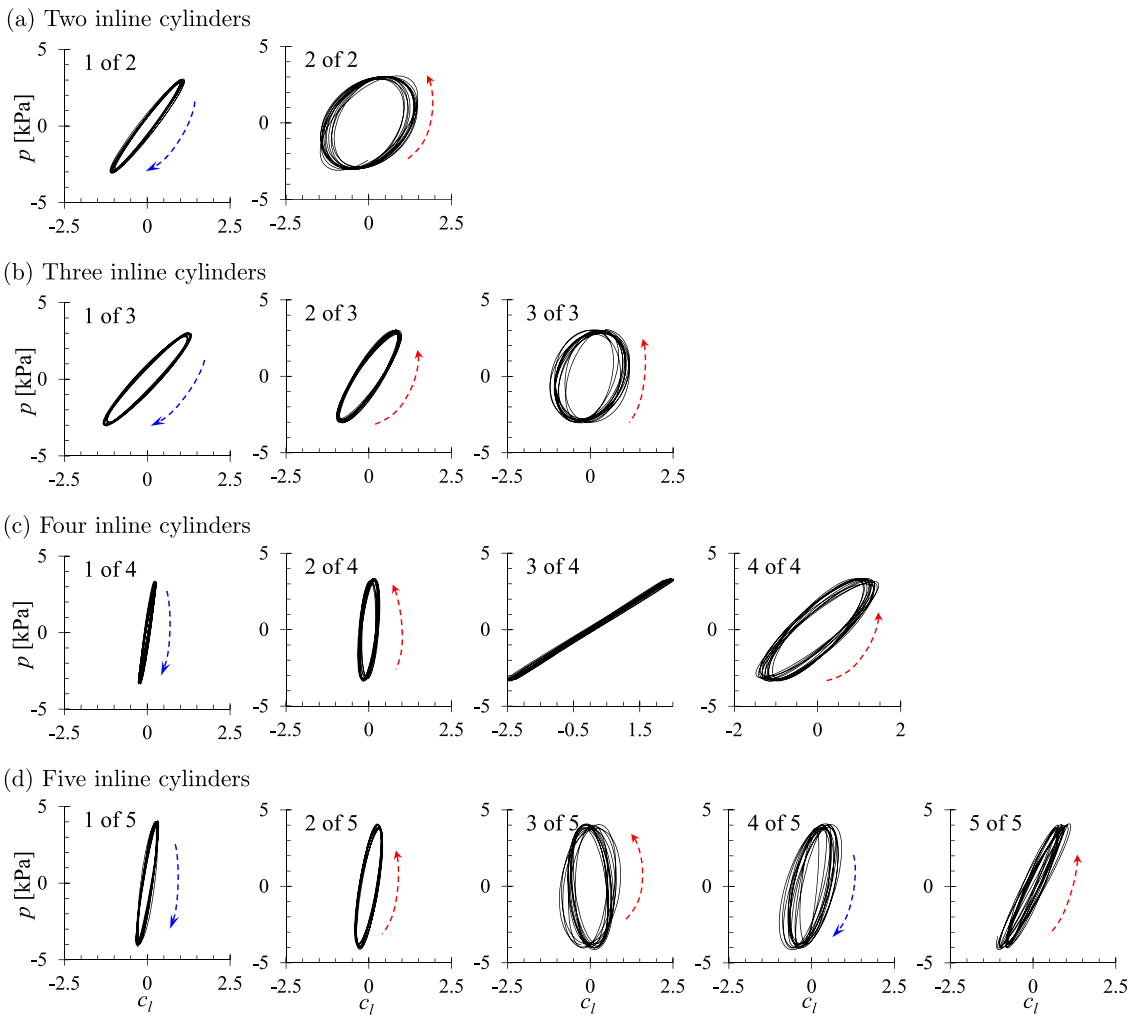


Fig. 11. Phase space of the acoustic pressure and the lift coefficients for inline arrangements of cylinders at the peak of acoustic resonance.

repeatable cycle, represented by a parabolic plot. Let the dynamic lift force on the cylinder be modeled as a driving force for the acoustic pressure oscillations. This entails that over an acoustic cycle, the work W done by the driving force on the acoustic particles displaced by d_a is equal to:

$$W = \int F_L d\,(d_a) \tag{5}$$

For the case of an acoustic standing wave, the acoustic pressure p at the pressure antinode is exactly in-phase with the acoustic particle displacement d_a at its antinode. Therefore, at a fixed frequency, the instantaneous value of the acoustic pressure measured at the top wall of the test section is proportional to the acoustic displacement in the plane of the cylinder axes, where the dynamic lift force is exerting work. As a result, the area inside the p-c_l loop represents the net work exerted by the dynamic lift force on the acoustic particle over the cycle. If the dynamic lift coefficient is higher at increasing values of p and lower at decreasing values of p, i.e. the cycle is counter-clockwise in the p-c_l space, the net work W is positive. A counter-clockwise cycle indicates a positive flow of energy from the flow field to the acoustic field. A clock-wise cycle direction is equivalent to the contrary, where the acoustic field would be damped by interactions at the surface of the cylinder.

Fig. 11 shows that the resonant system is in a stable condition, as expressed by the stable area of the cycles, although in some cases, the shape is not exactly repeatable. This suggests that the energy transfer from the flow field to the acoustic field is able to overcome the energy taken away from the acoustic field by acoustic damping and radiation to the far field, sustaining high pressure oscillations. Fig. 11 shows that the first two cylinders have consistent energy flow behavior in all configurations. For all configurations. the phase of the lift force with respect to the acoustic pressure on the upstream cylinder results in a negative energy flow that is limited in magnitude, as expressed by the relatively small cycle area. The

cylinders directly downstream of the upstream gap results in a positive energy flow for all investigated arrangements of cylinders. This consistency is related to the fact that the upstream gap flow should be similar in these configurations.

Another interesting observation is that the flow interaction with the surface of the most downstream cylinder for all configurations contributes positive energy to the acoustic field. The most downstream gap is affected similarly by the impinging shear layers in the gap and the downstream shedding field in all configurations. This is expected from the flow field in these gaps shown in Figs. 3–6. The flow in the most downstream gap is similar and consistent and unlike other gaps, shear layer impingement was not disrupted by gap flow.

It is interesting to see that the most upstream cylinder and the most downstream cylinder show opposite behavior in terms of energy transfer. The flow around the two cases is mirrored, in the sense that the most upstream cylinder is subject to separating flow on its upstream side, and vortices departing in the gap on its downstream side. The downstream cylinder on the other hand is subject to gap vortices impinging on its upstream side. Note that because the resonant field results in a pre-coincidence resonance, classical Von-Karman vortex shedding in the wake of the cylinders occurs at a frequency significantly lower than the dominant acoustic mode frequency considered here, and do not affect the interactions during resonance. It makes sense therefore to see the opposite direction of the energy exchange, and the difference in magnitude, as expressed by the difference in the cycle area, can be attributed to the growth of the fluctuations in the flow field as they occur further downstream (Shaaban and Mohany, 2018).

When the configuration of cylinders includes more gaps than two, Fig. 11 shows that flow interaction at the surfaces of some cylinders other than the upstream may contribute little or negative energy to the acoustic field. This is the case for the third cylinder in the arrangement of four cylinders, and the fourth cylinder in the arrangement of five cylinders. These two cylinders, both second-to-most downstream, are affected by fluctuating flow patterns that do not contribute positive energy to the acoustic field, which explains the limit imposed on the acoustic pressure amplitude as more cylinders were added. The main flow feature thought to cause this behavior is flow passing through these gaps disrupting impingement, as seen in Figs. 5 and 6. Therefore, it is evident that this limit is not imposed by increased acoustic radiation or external damping, but it is rather a result of intrinsic flow interactions related to each particular cylinder arrangement.

5. Dynamic lift decomposition on multiple inline cylinders

In the following discussion, the results are used to characterize the influence of acoustic resonance excitation on the fluid forces acting on individual cylinders in a row. According to Lighthill (1952), the sound observed by a distant observer and generated by unbounded flows with sound sources concentrated at one region, is dependent upon the fluctuation of stresses in the source region. The rearranged equations are an aeroacoustic analogy to the Navier–Stokes equation for an ideal fluid at the far field, where the fluctuation of the fluid density ρ can be expressed as

$$\frac{\partial^2 \rho}{\partial t^2} - c_0^2 \nabla^2 \rho = \frac{\partial^2}{\partial x_i \partial x_i} \left(T_{ij}\right) \tag{6}$$

where c_0 is the sound speed and T_{ij} is the stress tensor that takes into effect compressive stress, viscous stress, and turbulent stress. In the presence of rigid boundaries, Curle (1955) proved that flows at low Mach numbers produce noise in form of a dipole sound source representing the fluctuating force exerted on the fluid by the solid boundaries, where the difference between the free stream density ρ_0 and the local density ρ at a distance x from the source takes the simpler form

$$\rho - \rho_0 = \frac{1}{4\pi c_0^2} \frac{x_i}{x^2} \frac{\partial}{\partial t} F_i(t) \tag{7}$$

where $F_i(t)$ is the time dependent forces exerted by the solid boundary on the fluid.

As per Eqs. (3) and (4) and using the value of the phase angle φ, the instantaneous dynamic lift coefficient can be decomposed into orthogonal in-phase and out-of-phase components:

$$\begin{aligned} c_l(t) &= \left[c_l' \cos(\varphi)\right] \sin\left(2\pi f_v t\right) + \left[c_l' \sin(\varphi)\right] \cos\left(2\pi f_v t\right) \\ &= c_{mh} \sin(2\pi f_v t) - c_{dh} \cos(2\pi f_v t) \end{aligned} \tag{8}$$

The negative sign in Eq. (8) accounts for the fact that the energy exchange occurs due to the acoustic particle velocity vector, which is out of phase with the acoustic pressure vector for the standing-wave acoustic mode under consideration. This procedure is analogous to the formulation of Sarpkaya (1978) for flow-induced vibration systems, where the acoustic particle velocity is modeled similar to the displacement of the cylinder. This decomposition requires the measurement of the lift force and the acoustic pressure simultaneously on all cylinders in an inline arrangement. The component in-phase with the acoustic pressure, c_{mh} can then be expressed as in Eq. (9).

$$c_{mh} = c_l' \cos(\varphi) \tag{9}$$

The in-phase component quantifies the acoustic field moving with the flow momentum, equivalent to an added mass effect (Sarpkaya, 1978; Mohany, 2007). When the value of c_{mh} increase, the added inertia would mean the frequency

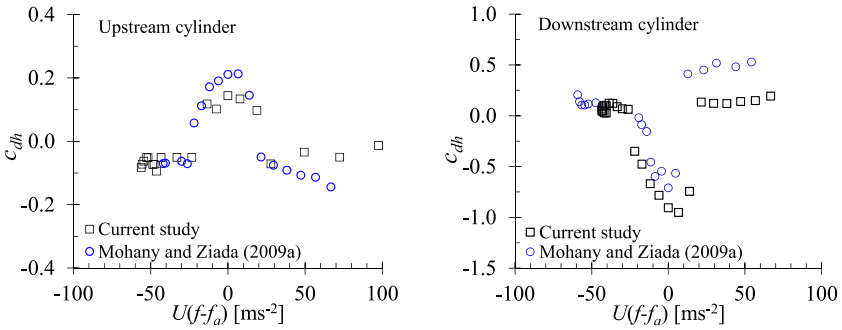


Fig. 12. Out-of-phase lift coefficient amplitude with respect to the acoustic pressure c_{dh} on the upstream and the downstream cylinders compared with the results of Mohany and Ziada (2009a) for the case of two tandem cylinders.

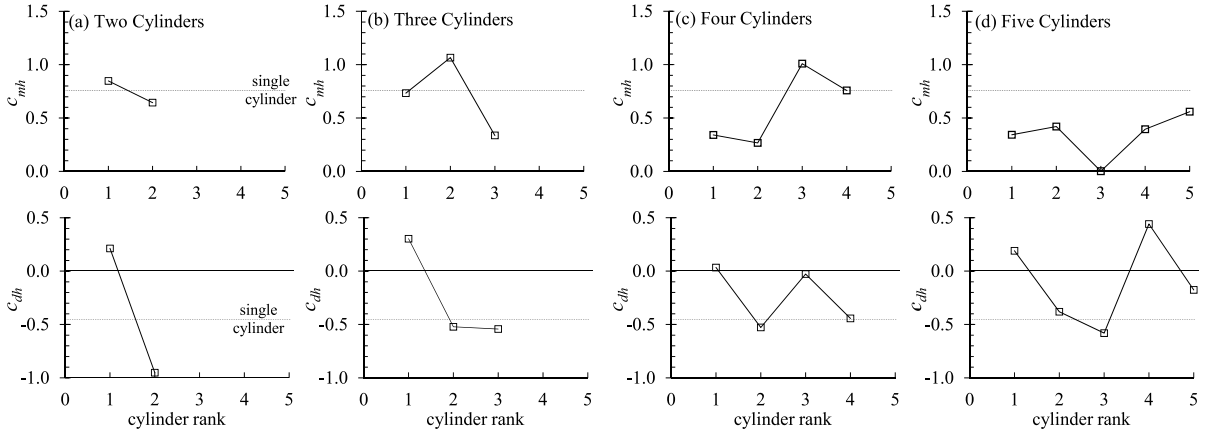


Fig. 13. The effect of the number of cylinders on the orthogonal dynamic lift components at the peak of pre-coincidence acoustic resonance.

of resonant oscillations is expected to be lower. The out-of phase component, c_{dh} defined in Eq. (10) quantifies energy exchange between acoustic and flow fields.

$$c_{dh} = -c_l' \sin(\varphi) \tag{10}$$

The component c_{dh} is analogous to an effect of added damping, where a positive value of c_{dh} indicates that the flow periodic instabilities are not expected to result in acoustic resonance, while a negative value of c_{dh} demonstrates that flow instabilities would grow and result in strong resonant conditions. The decomposed components of the dynamic lift coefficients are presented to investigate the energy transfer for each case, and the contribution of the different cylinders to the self excitation of a strong resonant acoustic field.

Fig. 12 shows the values of the out-of-phase component of the dynamic lift coefficients with respect to the acoustic field for two tandem cylinders. For measurements from the present study, the cylinders have a center-to-center spacing of $L/D = 2.00$, within the proximity interference region. The compared case from the study of Mohany and Ziada (2009a) has a spacing ratio $L/D = 1.75$, within the proximity interference region and expected to be influenced by the same flow structures. The two figures are plotted using the same axis selection of Fig. 8b to provide a scale-normalized comparison for the two cases. Fig. 12 shows good agreement of the out-of-phase component of the dynamic lift c_{dh} on the two cylinders before, during, and after the excitation of the pre-coincidence resonance. At the peak of resonance, the component c_{dh} is negative on the downstream cylinder during resonance, while slightly positive on the upstream cylinder for both cases. As noted by Mohany and Ziada (2009b), the negative component on the downstream cylinder indicates that the flow interaction with the downstream cylinder results in energy transfer from the flow field to the acoustic field, analogous to a negatively-damped system. Such system would be prone to a surge in acoustic pressure in form of acoustic resonance if excited by flow fluctuations.

To compare the decomposed components of the lift force as an indication of energy exchange for the four different cylinder configurations, Fig. 13 shows the values of the in-phase component c_{mh} and the out-of-phase component c_{dh} at the peak acoustic pressure of the pre-coincidence resonance. The cylinder rank is labeled starting from the most upstream cylinder. Dashed lines representing the values of c_{mh} and c_{dh} at the peak of the coincidence resonance for the case of a single cylinder of the same diameter for comparison. The in-phase component, equivalent to an added mass effect,

is positive for all cases, which suggests that the excitation of pre-coincidence resonance through dynamic flow forces would alter the normal resonance frequency of the surrounding duct. This can explain that pre-coincidence resonance for all cases locks in with a frequency of around 650 Hz, compared with the theoretical value of 674 Hz, a phenomenon that was reported for many other configurations.

The out-of-phase component c_{dh} in the lower set of Fig. 13 during resonance is equivalent to a damping effect that indicates that energy exchanged maintained by the dynamic lift force to sustain the pre-coincidence resonance. The upstream cylinder causes positive damping for all cases, indicating that flow structures around this cylinder are not contributing to the acoustic resonance. Instead, strong oscillations of the acoustic field result in the significant dynamic lift coefficient increase on the upstream cylinder. On the other hand, dynamic lift coefficient on cylinder 2 causes negative damping for all cases. The negative damping is highest for the case of two inline cylinders, and is nearly the same for the remaining cases. The cases with four inline cylinders, and five inline cylinders had the next-to-most-downstream cylinder with no or positive damping, which can be the result of complex interactions that was observed for rows with more cylinders. Such interactions include the disruption of the shear layer impingement on these cylinders by gap flow, and the distortion of the vorticity field by successive interaction with cylinders, as seen in Figs. 3–6. The flow distortions around the downstream cylinders result in less efficient energy exchange than the upstream cylinders. For all configurations, the absolute value of c_{dh} reaches its peak for cylinder 2, directly next to the upstream cylinder. As seen in the flow structures, this cylinder is the first cylinder that is subject to vortex impingement from the separating vortices upstream. The vortices are not yet distorted and are shed at a consistent rate and strength. The downstream cylinders, however, are subject to interaction with distorted vortices, which led to lower values of c_{dh} that can in some cases, turn positive, leading to no sensible increase in the strength of the excited acoustic resonance.

The behavior noted here can be extrapolated to explain the response of inline tube bundles where an increase in the number of cylinders does not lead to significant increase of strength of acoustic resonance. The first few rows of cylinders, where most of the periodic instabilities have been reliably identified are expected to dominate the self-excitation of resonance. Successive interaction between the flow structures and the array of cylinders would inhibit the regularity of the fluctuations and inject the flow energy into turbulent kinetic energy, leaving less energy to participate in acoustic energy production. The acoustic field may still be excited and effective around its localized source, leading to organized flow-sound interaction, but it is not expected that this regularity dominates the whole flow field. Therefore, countermeasures taken to prevent or mitigate the self-excitation of acoustic resonance in inline tube arrays should be aimed at disrupting or eliminating the regular vorticity and shear layer separation within gaps between the first few rows of cylinders. If successful in inhibiting self-excitation of resonance and lock-in, less organized separation downstream leaves significantly less potential for excitation of acoustic resonance.

6. Conclusion

The effect of the excitation of pre-coincidence acoustic resonance on the flow field and the dynamic lift forces on a row of inline cylinders has been investigated. Phase-locked particle image velocimetry and direct measurements of dynamic lift force on each individual cylinder in a configuration of two to five cylinders at a spacing ratio of $L/D = 2.0$ were used to identify the effect of the number of cylinders on the resonance excitation mechanism. For all configurations, excitation of acoustic resonance by the Rossiter-like instabilities in gaps between cylinders led to the excitation of acoustic resonance at the same upstream flow velocity and acoustic pressure level despite the increased number of gaps where coupling can potentially create sound sources. Acoustic resonance excitation occurred at around $U_\infty = 75$ m/s, and led to acoustic pressure levels of $P_{rms} = 2.0 - 2.4$ kPa, and showed characteristics similar to acoustic resonance observed in inline tube arrays. Particle image velocimetry revealed that increasing the number of cylinders led to interactions of the periodic flow structures with more downstream cylinders, leaving the flow structures more distorted, fragmented, and out of sync with the acoustic pressure cycle. Moreover, disruption of the shear layer impingement on the downstream cylinder of some gaps occurred as a result of gap flow in the configurations of four and five inline cylinders.

Dynamic lift on each cylinder in the row was measured simultaneously with the anti-node acoustic pressure signal using a custom setup that satisfies the high stiffness requirement needed for accurate measurements at the frequency of the acoustic mode $f_a = 654$ Hz. A notable change in the amplitude and phase of the dynamic lift force on all cylinders was observed at the self-excitation of acoustic resonance. The dynamic lift force on each cylinder was completely dominated by the acoustic resonance frequency, and the phase angle changed significantly. The phase between the dynamic lift force and the anti-node acoustic pressure was used to investigate the energy exchange characteristics around each cylinder during excitation of acoustic resonance. For all cylinders, a dynamic lift component equivalent to an added mass effect was contributed to by all cylinders, leading to a decrease in the acoustic mode frequency from its value for an empty duct. The dynamic lift force component that is equivalent to an added damping effect of resonance excitation had an overall negative value, and was prominently negative on most cylinders. However, the upstream cylinder and occasionally another cylinder downstream had no contribution to the excitation of acoustic resonance, suggesting that as the number of cylinders increases, less efficient acoustic energy production is expected to take place deep within an array of inline tubes. These observations suggest that designs for techniques or devices that aim to reduce or eliminate the excitation of acoustic resonance should target the formation of coherent periodic structures within the first few rows of cylinders in inline tube bundles, particularly the impingement of separating flow on cylinders in the second and third rows, which would disrupt the energy exchange at the acoustic mode frequency, and prevent pre-coincidence acoustic resonance excitation.

CRediT authorship contribution statement

Mahmoud Shaaban: Conceptualization, Methodology, Investigation, Formal analysis, Data curation, Writing - original draft. **Atef Mohany:** Supervision, Conceptualization, Writing - review & editing, Resources, Funding acquisition.

Declaration of competing interest

The authors declare that they have no known competing financial interests or personal relationships that could have appeared to influence the work reported in this paper.

Acknowledgment

The authors thankfully acknowledge the financial support provided by the Natural Sciences and Engineering Research Council of Canada (NSERC).

References

Alam, M.M., Moriya, M., Takai, K., Sakamoto, H., 2003. Fluctuating fluid forces acting on two circular cylinders in a tandem arrangement at a subcritical Reynolds number. J. Wind Eng. Ind. Aerodyn. 91 (1–2), 139–154.
Arafa, N., Mohany, A., 2015. Aeroacoustic response of a single cylinder with straight circular fins in cross-flow. J. Press. Vessel Technol. 137 (5).
Arafa, N., Mohany, A., 2016. Flow-excited acoustic resonance of isolated cylinders in cross-flow. J. Press. Vessel Technol. 138 (1).
Arafa, N., Mohany, A., 2019. Wake structures and acoustic resonance excitation of a single finned cylinder in cross-flow. J. Fluids Struct. 86, 70–93.
Arie, M., Kiya, M., Moriya, M., Mori, H., 1983. Pressure fluctuations on the surface of two circular cylinders in tandem arrangement. J. Fluids Eng. 105 (2), 161–166.
Arthurs, D., Ziada, S., 2012. Self-excited oscillations of a high-speed impinging planar jet. J. Fluids Struct. 34, 236–258.
Blevins, R.D., 1985. The effect of sound on vortex shedding from cylinders. J. Sound Vib. 92 (4), 455–470.
Blevins, R.D., Bressler, M.M., 1993. Experiments on acoustic resonance in heat exchanger tube bundles. J. Sound Vib. 164 (3), 503–533.
Chen, S., 1984. Guidelines for the instability flow velocity of tube arrays in crossflow. J. Sound Vib. 93 (3), 439–455.
Chen, Y.N., Sturchler, R., 1977. Flow-induced vibrations and noise in the pipe system with blind branches due to coupling of vortex shedding. In: INTER-NOISE and NOISE-CON Congress and Conference Proceedings, Vol. 2. Institute of Noise Control Engineering, pp. 438–452.
Curle, N., 1955. The influence of solid boundaries upon aerodynamic sound. Proc. R. Soc. Lond. Ser. A Math. Phys. Eng. Sci. 231 (1187), 505–514.
DeBoo, G., Ramsden, K., Gesior, R., 2006. Quad Cities Unit 2 main steam line acoustic source identification and load reduction. In: 14th International Conference on Nuclear Engineering. American Society of Mechanical Engineers, pp. 327–332.
Eisinger, F., Francis, J., Sullivan, R., 1996. Prediction of acoustic vibration in steam generator and heat exchanger tube banks. J. Press. Vessel Technol. 118 (2), 221–236.
Gu, F., Wang, J., Qiao, X., Huang, Z., 2012. Pressure distribution, fluctuating forces and vortex shedding behavior of circular cylinder with rotatable splitter plates. J. Fluids Struct. 28, 263–278.
Hong, Z., Wang, X., Jing, X., Sun, X., 2020. Frequency lock-in mechanism in flow-induced acoustic resonance of a cylinder in a flow duct. J. Fluid Mech. 884.
Inoue, O., Hatakeyama, N., 2002. Sound generation by a two-dimensional circular cylinder in a uniform flow. J. Fluid Mech. 471, 285–314.
Islam, M., Mohany, A., 2020. Vortex shedding characteristics in the wake of circular finned cylinders. Phys. Fluids 32 (4), 045113.
Karthik, B., Chakravarthy, S., Sujith, R., 2003. Jet forking driven by pipe tone. J. Acoust. Soc. Am. 113 (6), 3091–3094.
Koch, W., 2009. Acoustic resonances and trapped modes in annular plate cascades. J. Fluid Mech. 628, 155–180.
Lighthill, M.J., 1952. On sound generated aerodynamically. I. General theory. Proc. R. Soc. A 211 (1107), 564–587.
Liu, L., Feng, J., Wu, H., Xu, W., Tan, W., 2017. Fluid excitation forces on a tightly packed tube bundle subjected in cross-flow. J. Press. Vessel Technol. 139 (3), 031307.
Liu, X., Willeke, T., Herbst, F., Yang, J., Seume, J., 2018. A theory on the onset of acoustic resonance in a multistage compressor. J. Turbomach. 140 (8), 081003.
Mohany, A., 2007. Flow-Sound Interaction Mechanisms of a Single and Two Tandem Cylinders in Cross-Flow (Ph.D. thesis). McMaster University, ProQuest.
Mohany, A., Arthurs, D., Bolduc, M., Hassan, M., Ziada, S., 2014. Numerical and experimental investigation of flow-acoustic resonance of side-by-side cylinders in a duct. J. Fluids Struct. 48, 316–331.
Mohany, A., Ziada, S., 2005. Flow-excited acoustic resonance of two tandem cylinders in cross-flow. J. Fluids Struct. 21 (1), 103–119.
Mohany, A., Ziada, S., 2009a. Effect of acoustic resonance on the dynamic lift forces acting on two tandem cylinders in cross-flow. J. Fluids Struct. 25 (3), 461–478.
Mohany, A., Ziada, S., 2009b. Numerical simulation of the flow-sound interaction mechanisms of a single and two-tandem cylinders in cross-flow. J. Press. Vessel Technol. 131 (3), 031306.
Mohany, A., Ziada, S., 2011. Measurements of the dynamic lift force acting on a circular cylinder in cross-flow and exposed to acoustic resonance. J. Fluids Struct. 27 (8), 1149–1164.
Norberg, C., 2002. Pressure distributions around a circular cylinder in cross-flow. In: Proceedings of the Symposium on Bluff Body Wakes and Vortex-Induced Vibrations. pp. 1–4.
Norberg, C., 2003. Fluctuating lift on a circular cylinder: review and new measurements. J. Fluids Struct. 17 (1), 57–96.
Oengören, A., Ziada, S., 1998. An in-depth study of vortex shedding, acoustic resonance and turbulent forces in normal triangle tube arrays. J. Fluids Struct. 12 (6), 717–758.
Omer, A., Arafa, N., Mohany, A., Hassan, M., 2016a. The effect of upstream edge geometry on the acoustic resonance excitation in shallow rectangular cavities. Int. J. Aeroacoustics 15 (3), 253–275.
Omer, A., Mohany, A., Hassan, M., 2016b. Effect of impingement edge geometry on the acoustic resonance excitation and strouhal numbers in a ducted shallow cavity. Wind Struct. 23 (2), 91–107.
Oshkai, P., Velikorodny, A., 2013. Flow-acoustic coupling in coaxial side branch resonators with rectangular splitter plates. J. Fluids Struct. 38, 22–39.
Owen, P., 1965. Buffeting excitation of boiler tube vibration. J. Mech. Eng. Sci. 7 (4), 431–439.
Sarpkaya, T., 1978. Fluid Forces on Oscillating Cylinders, Vol. 78. NASA STI Recon Technical Report A, pp. 275–290.

Shaaban, M., Mohany, A., 2015. Passive control of flow-excited acoustic resonance in rectangular cavities using upstream mounted blocks. Exp. Fluids 56 (4), 56–72.
Shaaban, M., Mohany, A., 2018. Flow-induced vibration of three unevenly spaced in-line cylinders in cross-flow. J. Fluids Struct. 76, 367–383.
Shaaban, M., Mohany, A., 2019a. Characteristics of acoustic resonance excitation by flow around inline cylinders. J. Press. Vessel Technol. 141 (5).
Shaaban, M., Mohany, A., 2019b. Phase-resolved PIV measurements of flow over three unevenly spaced cylinders and its coupling with acoustic resonance. Exp. Fluids 60 (4), 71.
Szepessy, S., Bearman, P., 1993. Analysis of a pressure averaging device for measuring aerodynamic forces on a circular cylinder. Exp. Fluids 16 (2), 120–128.
Wang, P., Deng, Y., Liu, Y., 2019. Vortex dynamics during acoustic-mode transition in channel branches. Phys. Fluids 31 (8), 085109.
Wang, P., He, L., Liu, Y., 2020. Acoustics-driven vortex dynamics in channel branches with round intersections: Flow mode transition and three-dimensionality. Phys. Fluids 32 (2), 025101.
Wang, P., Liu, Y., 2019. Intensified flow dynamics by second-order acoustic standing-wave mode: vortex-excited acoustic resonances in channel branches. Phys. Fluids 31 (3), 035105.
Wang, P., Ma, H., Deng, Y., Liu, Y., 2018. Influence of vortex-excited acoustic resonance on flow dynamics in channel with coaxial side-branches. Phys. Fluids 30 (9), 095105.
West, G., Apelt, C., 1993. Measurements of fluctuating pressures and forces on a circular cylinder in the reynolds number range 10^4 to 2.5×10^5. J. Fluids Struct. 7.3, 227–244, available at (https://doi.org/10.1006/jfls.1993.1014).
West, G., Apelt, C., 1997. Fluctuating lift and drag forces on finite lengths of a circular cylinder in the subcritical reynolds number range. J. Fluids Struct. 11 (2), 135–158.
Ziada, S., 2006. Vorticity shedding and acoustic resonance in tube bundles. J. Braz. Soc. Mech. Sci. Eng. 28 (2), 186–189.
Ziada, S., 2010. Flow-excited acoustic resonance in industry. J. Press. Vessel Technol. 132 (1), 015001.
Ziada, S., Ng, H., Blake, C., 2003. Flow excited resonance of a confined shallow cavity in low Mach number flow and its control. J. Fluids Struct. 18 (1), 79–92.
Ziada, S., Oengören, A., 1992. Vorticity shedding and acoustic resonance in an in-line tube bundle part I: Vorticity shedding. J. Fluids Struct. 6 (3), 271–292.
Ziada, S., Oengören, A., 1993. Vortex shedding in an in-line tube bundle with large tube spacings. J. Fluids Struct. 7 (6), 661–687.